JOURNAL OF NEUROPHYSIOLOGY
Vol. 76, No. 3, September 1996. *Printed in U.S.A.*

Electrotonic Architecture of Hippocampal CA1 Pyramidal Neurons Based on Three-Dimensional Reconstructions

ZACHARY F. MAINEN, NICHOLAS T. CARNEVALE, ANTHONY M. ZADOR, BRENDA J. CLAIBORNE, AND THOMAS H. BROWN

Department of Psychology, Neuroengineering, and Neuroscience Center, and Department of Cellular and Molecular Physiology, Yale University, New Haven, Connecticut 06511; and Division of Life Sciences, University of Texas, San Antonio, Texas 78249

SUMMARY AND CONCLUSIONS

1. The spread of electrical signals in pyramidal neurons from the CA1 field of rat hippocampus was investigated through multicompartmental modeling based on three-dimensional morphometric reconstructions of four of these cells. These models were used to dissect the electrotonic architecture of these neurons, and to evaluate the equivalent cylinder approach that this laboratory and others have previously applied to them. Robustness of results was verified by the use of wide ranges of values of specific membrane resistance (R_m) and cytoplasmic resistivity.

2. The anatomy exhibited extreme departures from a key assumption of the equivalent cylinder model, the so-called "3/2 power law."

3. The compartmental models showed that the frequency distribution of steady-state electrotonic distances between the soma and the dendritic terminations was multimodal, with a large range and a sizeable coefficient of variation. This violated another central assumption of the equivalent cylinder model, namely, that all terminations are electrotonically equidistant from the soma. This finding, which was observed both for "centrifugal" (away from the soma) and "centripetal" (toward the soma) spread of electrical signals, indicates that the concept of an equivalent electrotonic length for the whole dendritic tree is not appropriate for these neurons.

4. The multiple peaks in the electrotonic distance distributions, whether for centrifugal or centripetal voltage transfer, were clearly related to the laminar organization of synaptic afferents in the CA1 region.

5. The results in the three preceding paragraphs reveal how little of the electrotonic architecture of these neurons is captured by a simple equivalent cylinder model. The multicompartmental model is more appropriate for exploring synaptic signaling and transient events in CA1 pyramidal neurons.

6. There was significant attenuation of synaptic potential, current, and charge as they spread from the dendritic tree to the soma. Charge suffered the least and voltage suffered the most attenuation. Attenuation depended weakly on R_m and strongly on synaptic location. Delay of time to peak was more distorted for voltage than for current and was more affected by R_m.

7. Adequate space clamp is not possible for most of the synapses on these cells. Application of a somatic voltage clamp had no significant effect on voltage transients in the subsynaptic membrane.

8. The possible existence of steep voltage gradients within the dendritic tree is consistent with the idea that there can be some degree of local processing and that different regions of the neuron may function semiautonomously. These spatial gradients are potentially relevant to synaptic plasticity in the hippocampus, and they also suggest caution in interpreting some neurophysiological results.

INTRODUCTION

The electrotonic structure of a neuron is important for several reasons. First, it is the basic platform on which much of the electrical signaling of the neuron is executed (Bekkers and Stevens 1990; Claiborne et al. 1992; Edwards et al. 1994; Hill et al. 1994; Holmes and Rall 1992a,b; Holmes et al. 1992; Jack et al. 1983; McKenna et al. 1992; Rall 1977). Second, it affects the extent of local information processing in various parts of the cell (Shepherd and Koch 1990; Shepherd et al. 1985, 1989). Third, it appears to play a role in voltage-dependent synaptic modifications that are thought to underlie certain types of learning (Brown et al. 1988a,b, 1991a,b, 1992). Fourth, understanding the cable properties of dendrites is important to the design and interpretation of studies of voltage-gated and synaptically mediated currents and potentials (Carnevale et al. 1994; Claiborne et al. 1992; Jaffe and Brown 1994; Johnston and Brown 1983; Kairiss et al. 1992; Spruston et al. 1993, 1994).

Previous studies have reported detailed compartmental models of pyramidal neurons in the visual cortex (Larkman et al. 1992) and hippocampal region CA3 (Major et al. 1994) as well as interneurons in hippocampal region CA1 (Thurbon et al. 1994). Here we focus on the electrotonic structure of pyramidal neurons from the CA1 region of the rat hippocampus. For studies of cellular neurophysiology and synaptic plasticity, these are among the most commonly used neurons of the mammalian brain (Brown and Zador 1990). They are the cells in which the "Hebbian" (Hebb 1949) nature of one form of long-term synaptic potentiation was first demonstrated (Kelso et al. 1986; Malinow and Miller 1986; Wigstrom et al. 1986). Because of the enormous amount of research being done on these cells, it is especially important to understand in considerable detail their electrotonic architecture and its implications both for neuronal function as well as for neurophysiological studies. The recent availability of three-dimensional morphometric reconstructions of hippocampal neurons (Amaral et al. 1990; Claiborne 1992; Claiborne et al. 1990, 1992; Ishizuka et al. 1995) combined with newer methods of electrotonic analysis and multicompartmental modeling (Claiborne et al. 1992; Hines 1984, 1989, 1993; Koch and Segev 1989; Mascagni 1989; Tsai et al. 1994b; Zador et al. 1995) enabled the new quantitative analysis we present here.

The results of this analysis also motivated us to present an examination of the appropriateness of the equivalent cylinder model of dendritic electrotonus and the inferences that it has generated. Our initial evaluation of hippocampal neurons from the CA1 region suggested that they are "electronically compact" (Brown et al. 1981), meaning that the steady-state electrotonic distance from the soma to the ends of the dendrites is not large. That study assumed that the cells could be reasonably approximated by a "ball and stick" model, in which the dendritic tree is represented by an equivalent cylinder (Holmes and Rall 1992a,b; Jack et al. 1983; Rall 1977; Rall et al. 1992). This assumption in turn rested on two implicit conditions. The first was that, for certain purposes, the entire dendritic arbor can be reasonably represented by a single uniform "equivalent" cylinder. The second was that one is interested only in "centrifugal" (Tsai et al. 1994b) voltage transfer; that is, transfer from the soma to the dendrites. In fact, one is usually also interested in "centripetal" voltage transfer; that is, transfer from the dendrites to the soma. In general these two voltage transfers tend to be very different (Brown et al. 1992; Carnevale and Johnston 1982; Rall and Rinzel 1973; Tsai et al. 1994b).

The results we present show that the equivalent cylinder model is not appropriate for CA1 pyramidal neurons; that the electrotonic architecture of these cells imposes severe constraints on the design and interpretation of neurophysiological studies; and that both centrifugal and centripetal current and voltage transfers should be considered in the analysis of electrotonic architecture.

METHODS

Dendritic morphology

NEURON LABELING. Pyramidal neurons in the CA1 region of the hippocampus were injected with horseradish peroxidase (HRP) with the use of techniques described previously (Claiborne et al. 1986, 1990; Rihn and Claiborne 1990). Briefly, male adult Sprague-Dawley rats were deeply anesthetized with Nembutal (60 mg/kg body weight) and decapitated. The brain was removed and 400-μm-thick slices of the middle third of the hippocampal formation were prepared and maintained at 32°C in a recording chamber (Claiborne et al. 1986). Pyramidal neurons in region CA1 were impaled with sharp electrodes filled with 2–3% HRP in KCl/tris(hydroxymethyl)aminomethane buffer (pH 7.6).

To decrease the chance of labeling cells whose dendrites had been severed during the slicing process, only somata located in the middle of the slice were impaled. Neurons with a resting potential of at least −60 mV were injected with HRP with the use of 3- to 5-nA positive current pulses with a duration of 250 ms at a rate of two per second for 20–25 min. After allowing 2–3 h for HRP diffusion, slices were fixed and processed with diaminobenzidine as described earlier (Claiborne et al. 1990). Importantly, the slices were left intact during tissue processing. To minimize shrinkage, the thick slices were cleared in ascending concentrations of glycerol and mounted on slides in 100% glycerol.

Slices treated in this manner shrink <5% in linear dimension, and the dendrites are not distorted (Claiborne 1992). Other methods of fixation and clearing do cause obvious shrinkage, both in the tissue itself and in neuronal processes. For example, if the slices are dehydrated with ethanol and cleared with xylene (as is done with thinner tissue sections, and often with Golgi-impregnated tissue), the filled dendrites become wrinkled. Water-based mounting media such as glycol methacrylate cause similar problems: as the media hardens over a period of days, the dendrites are gradually distorted. Given the small amount of tissue shrinkage observed with the methods we employed, no corrections for shrinkage were made.

THREE-DIMENSIONAL RECONSTRUCTION. Filled neurons were first drawn with the use of a camera lucida and a ×63 objective (Zeiss Neofluor oil-immersion lens; 0.5-mm working distance; numerical aperture = 1.25) attached to a Nikon Optiphot microscope. Only those cells that were well filled with HRP and had a minimum number of cut branches were analyzed further. Neurons were judged to be well filled if the staining was uniformly dense throughout the tree. If the dye appeared to fade toward the dendritic tips, the neuron was not included in the final sample. A neuron was also rejected if any primary dendrite was cut at the surface of the slice, or if >10 secondary or higher-order branches were severed. All four of the neurons included in the present study had <10 cut branches.

Dendritic trees that met these criteria were reconstructed in three dimensions directly from the thick slices with the use of a computer-microscope system designed by J. Miller (University of California, Berkeley), with software written by R. H. W. Nevin. The computer-microscope system has been described in detail elsewhere (Claiborne 1992; Jacobs and Nevin 1991; Nevin 1989). It consists of a Nikon Optiphot microscope with computer-controlled motors mounted on the stage and the focus-control knob. The stage is also equipped with optical encoders capable of 0.2 μm resolution. A video camera is mounted on the microscope and the dendrites are viewed on a monitor. Labeled neurons are digitized in three dimensions by an operator using a computer mouse.

Each data point consists of an X, Y, and Z coordinate and a diameter measurement. Diameter measurements are taken from a reference cursor that is superimposed over the dendrite on the monitor. Possible cursor diameters are limited by the pixel size of the video monitor and the magnification of the objective. Whenever the operator could not match the cursor diameter to the dendrite diameter, the next larger cursor diameter was chosen. Tests of this procedure found that it did not increase the surface area of dentate granule neurons by >14% (Rihn and Claiborne 1990). The four reconstructed neurons used in the present analysis consisted of between 3,000 and 4,000 data points, which included dendritic branchpoints and termination points. For tests of the "3/2 power branching rule," the daughter branch diameters were measured an average of 5.2 ± 2.2 μm from where the parent branch was measured.

Computer Simulations

SIMULATION PROGRAM. All simulations were performed on Sun SparcStations (model 2 or 10) with the use of NEURON (Hines 1984, 1989, 1993).

SPATIAL DISCRETIZATION. Digitized neuron morphologies were translated into NEURON syntax from the Neuron Tracing System (NTS) file format with the use of the program NTS-CABLE (J. Wathey, unpublished). Each unbranched dendritic segment was represented by one or more cylindrical "sections" of equivalent length and diameter. These sections were further subdivided into smaller "segments" with lengths no greater than 25 μm. This resulted in totals of 493–693 segments per dendritic tree. Somata were represented by a stack of six disks with diameters chosen by hand to conform to the original geometry.

TEMPORAL DISCRETIZATION. Membrane potentials were computed with NEURON's fully implicit backward-Euler integration method. Although this method is only first-order correct, in computations of steady-state values it is stable enough to give solutions in a single large time step (10^5 ms). In simulations involving dynamics of membrane potential or current, the time step was 0.1 ms.

TABLE 1. *Spine statistics*

Type	Diameter, μm	Length, μm	Area, μm^2	Density, μm^{-1}
Thin				2.0
Neck	0.10	0.50	0.21	
Head	0.25	0.50	0.40	
Mushroom				0.6
Neck	0.20	0.43	0.25	
Head	0.71	1.07	2.40	
Stubby	0.32	0.44	0.45	0.1
Total weighted spine area/length dendrite: 2.85 $\mu m^2/\mu m$				

From Harris et al. (1992).

SPINES. Because spine locations were not recorded during the digitization process, estimates of spine shape and density were based on serial electron microscope reconstructions of sampled adult rat hippocampal CA1-region neuropil by Harris and coworkers (Harris and Stevens 1989; Harris et al. 1992). They reported three main classes of spine morphology—"thin," "mushroom," and "stubby" (Harris et al. 1992). The respective spine dimensions and density of occurrence on dendritic processes are summarized in Table 1. All active synapses were placed at the end of thin spines, composed of single-compartment head and neck sections.

To account for the effect of inactive spines on cell electrical properties, we incorporated additional membrane area rather than explicitly modeling each spine. This method, which decreases R_m and increases membrane capacitance (C_m) in proportion to the increase in area, is quite accurate in direct comparisons with models in which spines were explicitly represented (Cauller and Connors 1992; Claiborne et al. 1992; Stratford et al. 1989). The figures from the work of Harris give an average cumulative spine area of 2.85 μm^2 per μm of dendrite length. This spine area was taken to be constant throughout the arbor, resulting in a 52% average increase in total membrane area for each cell.

SYNAPTIC CONDUCTANCES. Synaptic events were modeled by a time-dependent conductance in the form of a two-exponential function

$$g_{syn}(t) = \bar{g}_{syn} \frac{\tau_1 \tau_2}{\tau_1 - \tau_2} (e^{-t/\tau_1} - e^{-t/\tau_2}) \quad (1)$$

where $\tau_1 = 0.2$ ms is the rise time constant, $\tau_2 = 2$ ms is the decay time constant, and $\bar{g}_{syn} = 12.9$ nS (cf. Jonas et al. 1993; Xiang et al. 1994). These values give a waveform with a peak conductance of 2 nS and a total rise time of 0.512 ms, corresponding to a "20–80" rise time of 0.18 ms and a "10–90" rise time of 0.27 ms. The actual rise times are unknown in CA1. Rise times this fast or faster have been seen in perirhinal cortex (Faulkner et al. 1994), visual cortex (Stern et al. 1992), cochlear nucleus (Trussel et al. 1993), and cerebellar granule cells (Silver et al. 1992). Synaptic current was given by

$$I_{syn} = g_{syn}(V_{syn} - E_{syn}) \quad (2)$$

where V_{syn} is local membrane potential and $E_{syn} = 0$ mV is the synaptic reversal potential. Synaptic conductances were always applied to the head of a spine, as described above, rather than being placed directly on the dendritic shaft.

PASSIVE ELECTRICAL PARAMETERS. The electrical parameters used in these simulations were (see Table 2): specific $R_m = 10$–150 kΩ cm^2; specific $C_m = 1$ μF/cm^2; cytoplasmic resistivity (R_i) = 50–400 Ω cm. These values bracketed ranges suggested by sharp-electrode recordings (Barrionuevo and Brown 1983; Barrionuevo et al. 1986; Brown et al. 1981) and perforated-patch recordings (Spruston and Johnston 1992). In most cases repeated simulations were performed to explore the effects of changing parameters over these ranges. When not otherwise noted, midrange values were used. Parameter selection is discussed further in the section on calibrating the morphometrically derived compartmental model.

These estimates of R_m, C_m, and R_i are based on experiments in which voltage-gated ionic channels were neither inactivated nor blocked, and changes of membrane potential were small. The experimental observations therefore automatically included linear approximations of the effects of all active conductances that were present in the vicinity of the recording electrode. Consequently the electrical parameters are not in the strict sense "passive" but instead might be more accurately described as "linearized." Thus, even though we did not explicitly build active currents into our models, their effects on fluctuations within ~5 mV of resting potential are implicitly included. Nonlinearities associated with excursions outside this range are considered in the DISCUSSION.

ACTIVE CONDUCTANCES. Most simulations included passive membrane properties only. One set of simulations included voltage-dependent conductances in the soma. In this case, modified Hodgkin-Huxley type fast Na^+ and K^+ currents (Hodgkin and Huxley 1952) were represented with the use of a standard kinetic scheme (adapted from Traub and Miles 1991)

$$I_{HH} = \bar{g}_{Na} m^3 h (V - E_{Na}) + \bar{g}_K n^4 (V - E_K) \quad (3)$$

with state variables m, n, and h governed by differential equations of the form $\dot{x} = [x_\infty(V) - x]/\tau_x(V)$, where $\tau_x(V) = 1/[\alpha_x(V) + \beta_x(V)]$ and $x_\infty(V) = \alpha_x(V)\tau_x(V)$. The voltage dependencies of α and β for each of the state variables are given in Table 3. Here $\bar{g}_{Na} = 150$ μS/cm^2, $E_{Na} = 50$ mV, $\bar{g}_K = 500$ μS/cm^2, and $E_K = -90$ mV.

ELECTROTONIC MEASUREMENTS. Some of the early electrophysiological studies of hippocampal neurons (Brown et al. 1981; Johnston 1981) estimated the dendritic electrotonic length L from somatic recordings of charging curves. We did not use these methods because their susceptibility to noise (Aubard et al. 1987; Yeramian and Claverie 1987) could make the results obtained from real data and simulated charging curves quite different. Instead, we evaluated electrotonic distances based on steady-state attenuations. The steady-state voltage at any point along a finite cable with a "sealed end" boundary condition is given by Rall (1977)

$$V = V_0 \frac{\cosh(L - X)}{\cosh(L)} \quad (4)$$

where V_0 is the voltage at the origin, L denotes the location of the sealed end, and X is the electrotonic distance to any point along cylinder. For the special case in which $X = L$, *Eq. 4* reduces to

$$X \equiv \operatorname{arccosh}\left(\frac{V_0}{V_t}\right) \quad (5)$$

where V_t is the voltage at the termination of a dendritic branch.

This measure assumes that—in terms of voltage transfer from the soma to the tips of the dendrites—the entire dendritic tree can be collapsed into an equivalent, nontapering cylinder. There are

TABLE 2. *Electrical parameters*

Property	Symbol	Usual Value	Range	Unit
Specific membrane capacitance	C_m	1		μF/cm^2
Specific membrane resistivity	R_m	30	10–150	kΩ cm^2
Axial resistivity	R_i	200	50–400	Ω cm
Leak reversal potential	E_l	−60		mV

TABLE 3. *Hodgkin-Huxley state variable equations and parameters*

I_{Na}		I_K
m	h	n
$\alpha_m(V) = \frac{0.32(13 - V - E_l)}{e^{(13-V-E_l)/4} - 1}$	$\alpha_h(V) = 0.128e^{(17-V+E_l)/18}$	$\alpha_n(V) = \frac{0.032(15 - V - E_l)}{e^{(15-V+E_l)/5} - 1}$
$\beta_m(V) = \frac{0.28(V - E_l - 40)}{e^{(V-E_l-40)/5} - 1}$	$\beta_h(V) = \frac{4}{1 + e^{(40-V-E_l)/5}}$	$\beta_n(V) = 0.5e^{(10-V+E_l)/40}$

Leak reversal potential (E_l) = −60 mV.

several implications of this assumption, a key one being that each branch terminate at the same electrotonic distance from the soma. According to this conventional measure of electrotonic distance, voltage decays by $1/e$ for every unit of X in the case of an infinite or semi-infinite cylinder, but it suffers less decay in the case of a finite cylinder terminated in an open circuit (Rall 1977).

Elsewhere (Brown et al. 1992; Carnevale et al. 1995a,b; Tsai et al. 1993, 1994b; Zador et al. 1995) we suggest a new measure of electrical distance

$$L \equiv ln\left(\frac{V_0}{V_t}\right) \quad (6)$$

where the terms have their usual meanings. The motivation for this new definition was to free the measure of electrotonic distance from any restrictions on cellular geometry. Like the two-port theoretical approach (Carnevale and Johnston 1982; Carnevale and Lebeda 1987), which abandoned the classical electrotonic distance and instead focused on the efficacy of signal transfer, our new definition makes no assumptions about the appropriateness of the equivalent cylinder model. In what follows, for the sake of clarity we use X for *Eq. 5* and L for *Eq. 6* (more generally, we use the symbol L_{ij} for the electrical distance from i to j based on *Eq. 6*).

In contrast to the usual definition, our measure (*Eq. 6*) has the characteristic that voltage always decays by $1/e$ for every unit of L—regardless of whether or not the geometry is cylindrical, infinite, or unbranched. This intuitive and model-independent measure of electrical distance—lends itself nicely to graphical interpretations of both steady-state and transient electrotonic structure (Brown et al. 1992; Carnevale et al. 1995a,b; Tsai et al. 1993, 1994b; Zador et al. 1995). In what follows, we use both *Eqs. 5* and *6*.

RESULTS

Three-dimensional dendritic morphology

Even though we specifically attempted to inject cells located in the middle of the slice, most of the dye-filled neurons suffered too much dendritic loss to be included in this study. Our selection criteria for complete dendritic trees rejected ~60% of the injected cells. For the present analysis, four cells that were judged to be representative of the population of CA1 pyramidal neurons satisfied our selection criteria for dendritic integrity. Figure 1 illustrates the reconstructed morphologies of these cells.

The dendritic trees were qualitatively and quantitatively similar to those described previously (Amaral et al. 1990; Ishizuka et al. 1995; Lorente de Nó 1934). All neurons had one primary apical dendrite that emerged from the apex of the soma toward the stratum radiatum. In two cells [Fig. 1*A* (*cell 503*) and Fig. 1*C* (*cell 822*)], this trunk bifurcated in stratum radiatum into two branches of approximately equal diameter. The primary apical did not bifurcate in the other two neurons [Fig. 1*B* (*cell 602*) and Fig. 1*D* (*cell 913*)]. In all four neurons the primary apical dendrites reached the hippocampal fissure, sometimes curving and traveling along the fissure for several hundred micrometers before terminating. Secondary and higher-order segments were visible along the entire length of the primary apical. The basal dendritic trees were similar in all of the neurons. From three to five basal dendrites extended from the cell body toward the alveus. Each gave rise to higher-order branches. Both apical and basal dendrites were covered with spines.

These cells had an average of 113 apical branches (range 93–148), an average of 42 basal branches (range 29–51), and an average total dendritic length of 12,586 μm (range = 10,555–14,708). Table 4 summarizes additional morphometric data on these four cells. The average total dendritic length we observed is similar to the findings of others (Amaral et al. 1990; Ishizuka et al. 1995); Ishizuka et al. (1995) reported a value of 13,424 μm for 23 HRP-filled pyramidal neurons from the CA1 region of rat hippocampus.

Different processes terminated at very different distances from the soma. The distribution of anatomic distances from the soma to the tips of each of the dendrites is illustrated in Fig. 2. In all four cells, the probability density functions of anatomic distance had at least two prominent peaks—one at 200–350 μm and another at 600–850 μm. There was considerable variability and the coefficient of variation (CV) was large (0.43–0.61; see legend to Fig. 2).

BRANCHPOINT DIAMETER COEFFICIENTS. One requirement for a dendritic tree to be reducible to an equivalent cylinder is the so-called 3/2 power rule, according to which the 3/2 power of the diameter of each parent branch equals the sum of the 3/2 powers of the diameters of the daughter branches (Rall 1977). To test this assumption we defined the "branchpoint diameter coefficient" (BDC) as the ratio of the 3/2 power of the parent diameter to the sum of the 3/2 powers of the daughter diameters. The equivalent cylinder model asserts that the BDC is unity and has no variance about this value.

The distribution of BDCs is illustrated for all four cells in Fig. 3 (solid lines). The vertical line marks the predicted result (a spike centered at 1.0). Most of the BDCs were in the range of 0.4–0.7, with relatively few reaching the assumed value of 1.0. In addition, the distributions tended to be multimodal and had large CVs. The fact that the distributions fell far to the left of the expected value indicates that the combined daughter branches tend to be too large relative to the parent branch. Consequently centrifugal voltage atten-

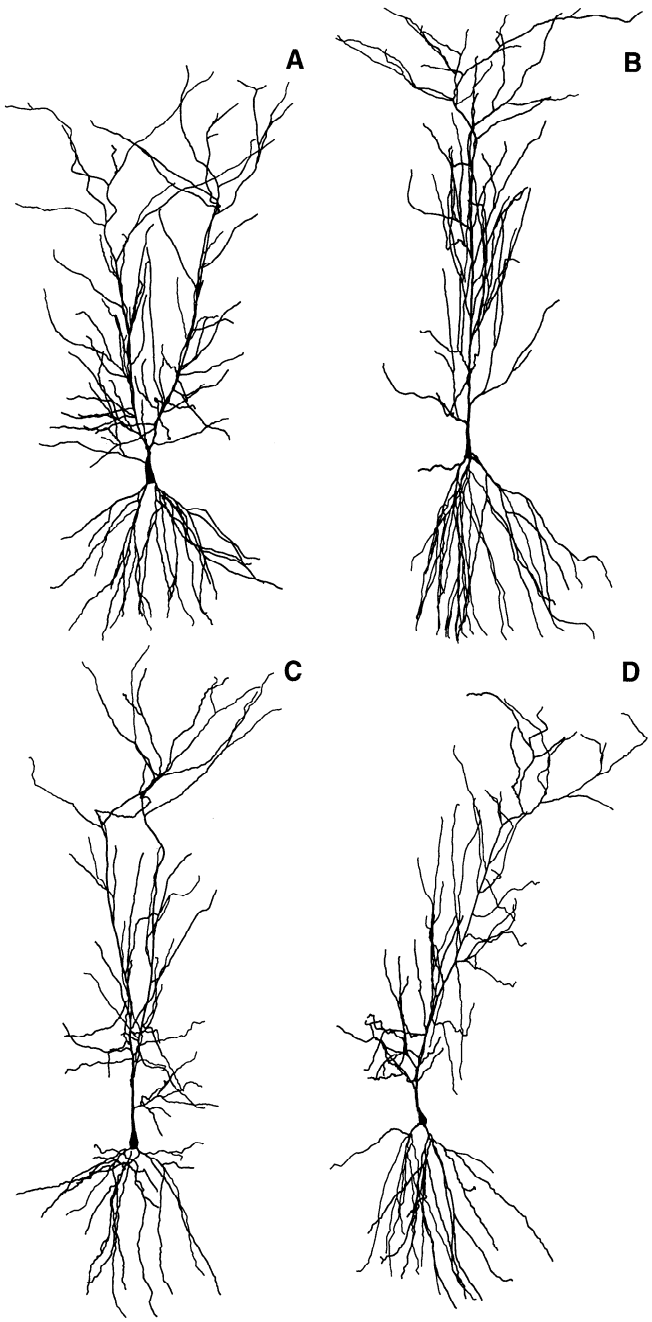

FIG. 1. Two-dimensional projections of the 4 reconstructed hippocampal CA1 pyramidal neurons. Two of the cells [*A* (*cell 503*) and *C* (*cell 822*)] had a bifurcating apical dendrite and 2 [*B* (*cell 602*) and *D* (*cell 913*)] had a nonbifurcating apical dendrite. These cells, which were selected by strict criteria for dendritic integrity, were judged to be representative of the population of CA1 pyramids.

uation is greater, and centripetal attenuation is less, than would be expected if the BDCs clustered around 1.0. The large CVs and multimodal distributions suggest that no simple alternative to the 3/2 power rule adequately captures the anatomy. Because of indications that diameters may have been overestimated (see *Calibrating the multicompartmental models,* below), we reduced the diameters by 0.5 μm and repeated the BDC calculations (Fig. 3, dotted lines). The diameter correction accentuated the peaks and increased the CVs.

Calibrating the multicompartmental models

Now we turn our attention to the problem of calibrating the morphometrically derived compartmental model (Claiborne et al. 1992; Perkel and Mulloney 1978; Rall et al. 1992). Specifically, one would like to restrict the range of possible electrical constants and to evaluate the extent to which various sets of assumed parameters are internally consistent given the best experimental estimates of the physiology of these neurons.

INPUT RESISTANCE AND R_m. The most obvious consistency test concerns the input resistance (R_N). This was calculated from the steady-state voltage response to a current step injected into the soma of each of the four model cells. This computation was repeated for values of specific R_m from 10 to 50 kΩ cm^2 and values of R_i from 50 to 400 Ω cm. Results of 160 simulations performed on all four cells are shown in Fig. 4. Increasing R_m or R_i increased R_N. The sets of nearly parallel lines in Fig. 4, *A–D,* represent different values of R_i, with lower values at the *bottom.* Within the range of parameter values that we explored, there was a slightly nonlinear relationship between R_N and R_m. This nonlinearity decreased as R_i decreased. The effects of R_i on R_N are shown in Fig. 4, *E–H,* where the lowest values of R_m are at the *bottom.*

The R_Ns of the models are certainly consistent with the ranges that this laboratory has found with the use of sharp electrodes (Barrionuevo et al. 1986; Brown et al. 1981; Kelso et al. 1986). However, we now know that the experimentally measured R_N depends on the recording method (Claiborne et al. 1992; Spruston and Johnston 1992; Staley et al. 1992). Sharp electrodes yield lower values and whole cell recordings give higher values. Unfortunately, the correct value is still somewhat uncertain.

If C_m is taken to be a biological constant (1 μF/cm^2) (Brown et al. 1981; Jack et al. 1983; Johnston 1981), then R_m should be ~30 kΩ cm^2 (because membrane time constant = C_mR_m). Assuming a conventional value of R_i = 200 Ω cm yields the following R_Ns in our models: 36 MΩ (*cell 503*), 39 MΩ (*cell 602*), 48 MΩ (*cell 822*), and 49 MΩ (*cell 913*), for an average value of 43 MΩ. These R_N values are smaller than one would expect given the results of whole cell measurements from hippocampal CA1 pyramidal neurons in guinea pig with the use of the nystatin patch method (Spruston and Johnston 1992). The observations of Spruston and Johnston suggest an average R_N of ~100 MΩ and an average membrane time constant of ~30 ms. Similar experiments have not been reported for rat, but these values can serve as estimates.

POSSIBLE CAUSES OF APPARENT DISPARITY. There are several possible causes of this apparent disparity between our results and those of Spruston and Johnston (1992). Recent studies have indicated that R_i might be >200 Ω cm, and some investigators have suggested values as high as 300 or 400 Ω cm (Major et al. 1994; Thurbon et al. 1994). Increasing R_i from 200 to 400 Ω/cm does increase R_N, but it does not double the value (Fig. 4, *E–H*). Another possibility is that the process diameters were overestimated by more than our previous work suggested (Rihn and Claiborne 1990). Indeed, recent evidence from confocal scanning laser microscope measurements suggests that this is the case (O'Boyle

TABLE 4. *Morphological parameters*

	Cell				
	503	*602*	*822*	*913*	Mean
Dendritic length, μm	14,708	13,627	11,452	10,555	12,586
Dendritic area, μm^2	80,959	79,735	62,367	61,807	71,217
After correction,* μm^2	57,853	55,977	44,377	42,577	50,196
Spine area,† μm^2	41,183	38,155	32,065	29,552	35,238
Soma area, μm^2	1,182	715	897	522	829
Number of apical branches	148	107	93	105	113
Number of basal branches	51	46	43	29	42

* Dendritic area after correction incorporate 0.5 μm diameter reduction (see text). † Spine areas are calculated from data in Harris et al. (1992).

et al. 1993). Decreasing the process diameters by as little as 0.5 μm (which is within the range of bias) increased R_N in the four cells by 55–62%.

A third possibility is that our morphometrically reconstructed cells have fewer cut dendrites than is typical of the cells recorded by Spruston and Johnston (1992). As indicated in METHODS, we took great pains to reduce the number of cut dendritic processes and analyze only cells with a minimum number of cut dendrites. Thus the two populations of neurons—ours and those of Spruston and Johnston (1992)—may have included different fractions of the dendritic arbor. To explore this possibility further, we evaluated the effect on R_N of truncating the dendritic arbor in the four model cells. Planes at varying distances above the soma were used to truncate the dendritic tree. Results of this pruning are summarized in Fig. 5, *A–D*. It is clear that if one tends to record mainly from neurons whose somata are near the surface of the slice, which is common when patch pipette methods are used, then dendritic pruning could have a major effect on the measured R_N.

Finally, we should note that there may be species differences. Spruston and Johnston (1992) worked with guinea pigs, whereas our morphometry was from rats (both studies were of adult animals).

It is clear that several factors could reduce or eliminate the apparent discrepancy between our results and those of Spruston and Johnston. Pending a resolution, in subsequent sections we assumed the following as a first approximation: R_i = 200 Ω cm and R_m = 30 kΩ cm^2; all diameters were corrected by subtracting 0.5 μm; and the dendritic trees were not pruned. This changed the R_Ns in the four cells to the following values: 51 MΩ (*cell 503*), 57 MΩ (*cell 602*), 69 MΩ (*cell 822*), 88 MΩ (*cell 913*), giving a mean value of 66 MΩ. We also continued to perform parametric variations to ensure that the results were robust. None of the following results were qualitatively different if one assumed alternative

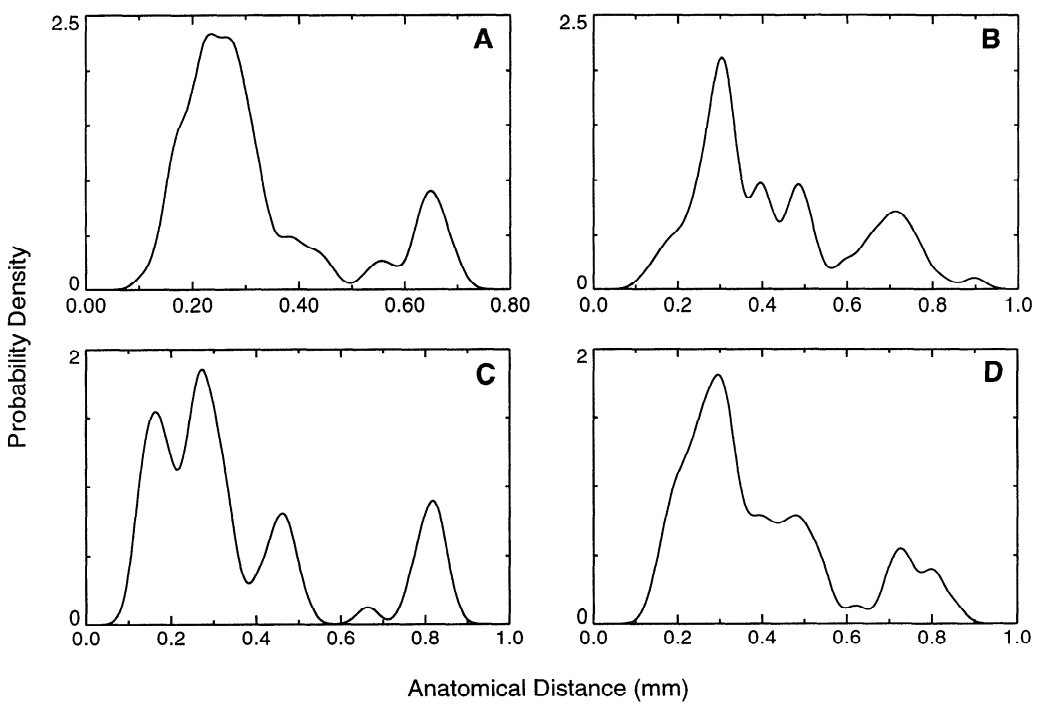

FIG. 2. Distributions of anatomic distances from somata to dendritic tips. *A–D* correspond to the neurons illustrated in Fig. 1. Probability densities were generated by Gaussian smoothing of the relative frequency distribution of anatomic distances. The Gaussian kernel had SD (σ) of either 20 μm (*A*) or 25 μm (*B–D*). The distributions were multimodal with large coefficients of variation (CV = SD/mean; CV_A = 0.49, CV_B = 0.43, CV_C = 0.61, and CV_D = 0.47).

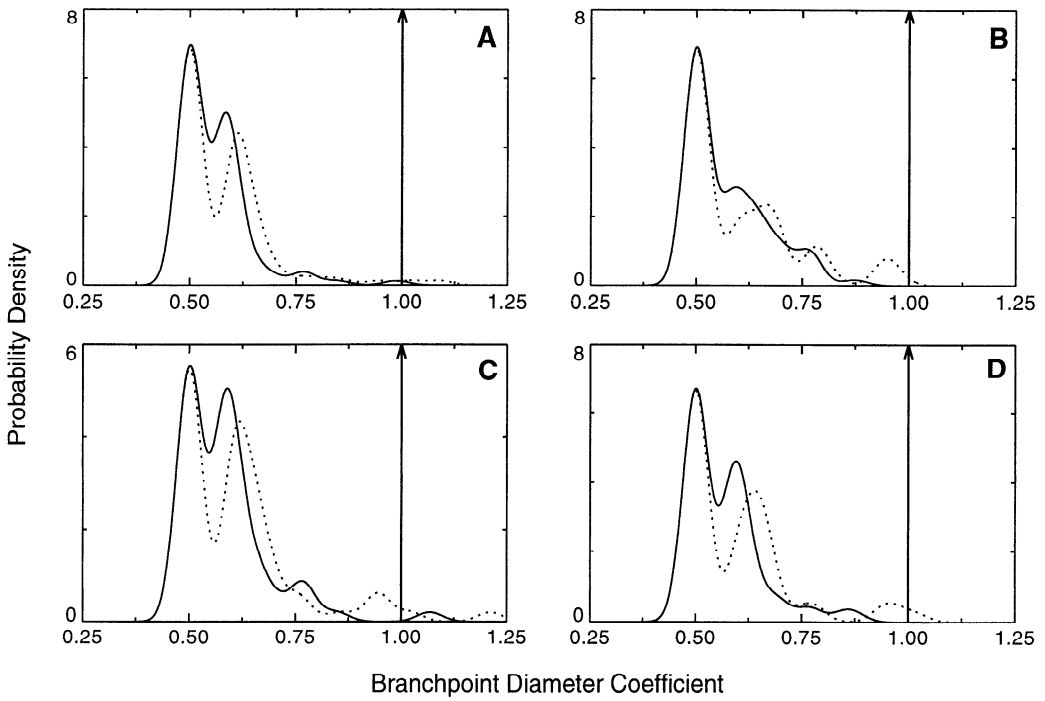

FIG. 3. Distribution of branchpoint diameter coefficients (BDCs). BDC is defined as $\mathrm{Diam_p^{3/2}}/\sum_d \mathrm{Diam_d^{3/2}}$, where $\mathrm{Diam_p}$ is the diameter of the parent branch and $\mathrm{Diam_d}$ are diameters of the daughter branches. The equivalent cylinder model demands a BDC of 1.0 for all branchpoints. Solid and dotted lines: BDC distributions with and without 0.5 μm diameter corrections (see text). *A–D*: probability densities of BDCs for the corresponding cells in Fig. 1. For each cell, the distribution lies well to the left of 1.0 (vertical line) is multimodal, and has a sizeable CV (average 0.16 before and 0.21 after diameter correction). The smoothed distributions were generated as described in Fig. 2, with $\sigma = 0.03$.

model parameters within the ranges that were discussed thus far.

Electrotonic structure of the dendritic arbor

VOLTAGE TRANSFER AWAY FROM SOMA. According to the equivalent cylinder model of dendritic electrotonus, the steady-state attenuation of voltage spreading from the soma to each dendritic tip should be identical. We tested this assumption by computing these attenuations from anatomically based multicompartmental models. Then for each dendritic termination we found the corresponding "classical electrotonic distance" X (*Eq. 5,* based on the equivalent cylinder approach) and our "new electrotonic distance" L (*Eq. 6,* which does not depend on the equivalent cylinder model). If the equivalent cylinder model is applicable, then the frequency distributions of X and L values should both show a single peak with essentially no variance ($\sigma_X^2 = \sigma_L^2 = 0$).

The results sharply contradicted this prediction (Fig. 6, *A–D,* and Table 5). In all four cells, the distributions of X (· · ·) and L (——) were multimodal and had large CVs. As expected, for each dendritic termination L was smaller than the corresponding X, because voltage decays by $1/e$ for every unit of L (by definition) but decays by less than $1/e$ for every unit of X in a finite cylinder.

This outcome was qualitatively the same with and without the 0.5 μm diameter reduction to correct for a possible size overestimate (see *Calibrating the multicompartmental models,* above). The effect of the diameter correction was to accentuate the peaks and increase the CV.

These findings were not specific to particular assumed values of R_m and R_i, but held up over a wide range of variation of both of these parameters as illustrated in Fig. 6, *E* and *F* (*cell 822,* morphology shown in Fig. 1*C*). The distributions showed more peaks and a larger range as R_m decreased and as R_i increased.

The results presented in Figs. 3 and 6 and Table 5 clearly indicate that these dendrites cannot be adequately represented by an equivalent cylinder.

RELATIONSHIP OF PEAKS TO LAMINAE. The multimodal distribution of L values (Fig. 6) raised the question of their relationships to the various laminae in the hippocampus. To explore this relationship, the dendritic processes were subdivided into the following three groups, according to the layer in which they terminated (Fig. 7): stratum oriens (basilar dendrites), stratum radiatum (proximal apical dendrites), and stratum lacunosum-moleculare (distal apical dendrites receiving innervation from the perforant pathway). The separation between stratum radiatum and stratum lacunosum-moleculare is visually apparent from the characteristic bending of the dendrites at the beginning of stratum lacunosum-moleculare. The frequency distributions of L were then determined and Gaussian-smoothed histograms were plotted separately for the three groups. As indicated (Fig. 7, *A–D*), the distributions were quite different for dendrites terminating in the three strata.

In all four cells, the distribution of L for terminations in stratum oriens was unimodal and had the smallest mean. The distribution of L for terminations in stratum lacunosum-moleculare had a single major peak and the largest mean.

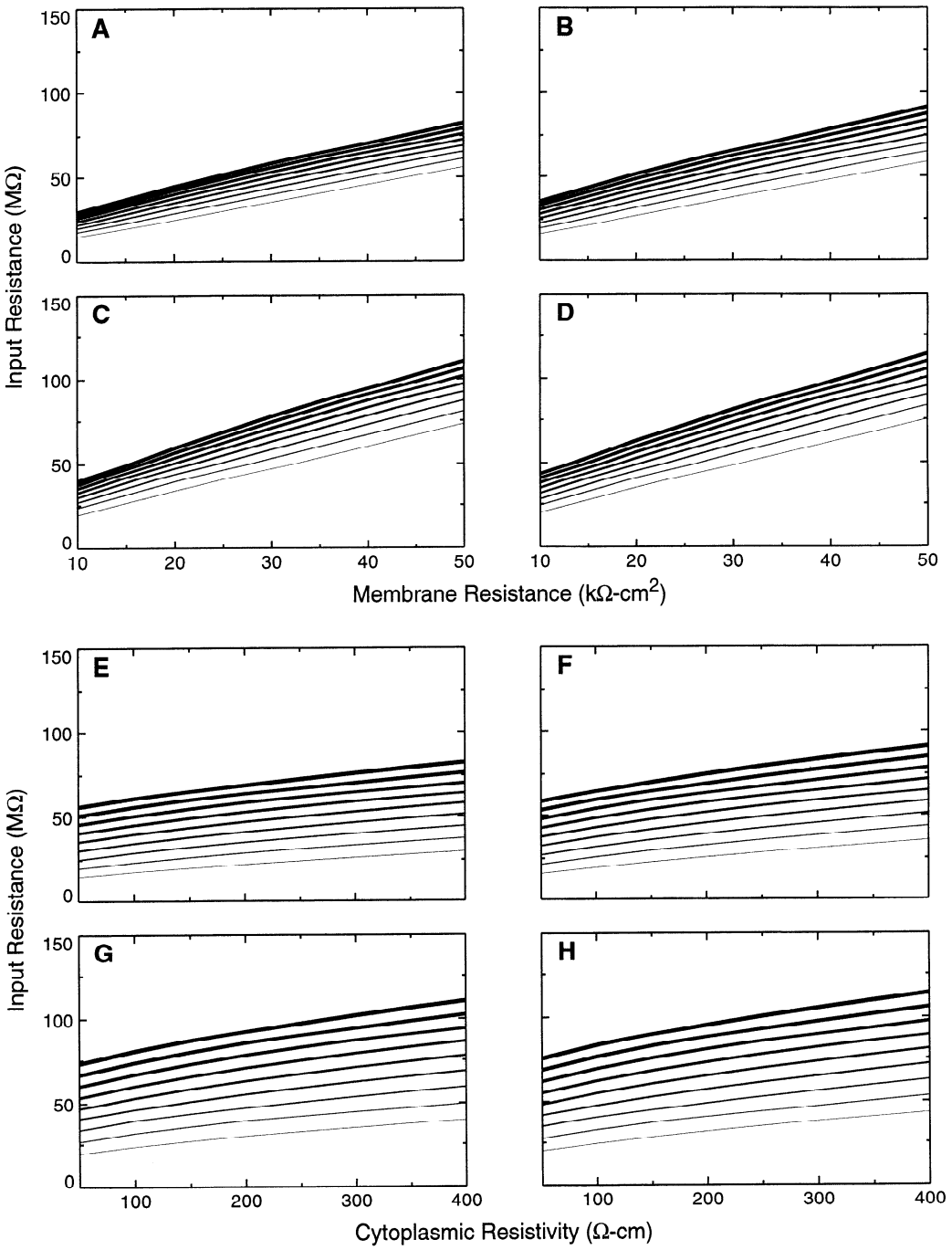

FIG. 4. Input resistance (R_N) as a function of electrical parameters. *A–D*: R_N for models of the 4 CA1 neurons of Fig. 1 is plotted as a function of specific membrane resistance (R_m = 10–50, kΩ cm^2), with different curves corresponding to different values of cytoplasmic resistivity (R_i = 50, 100, 150, 200, 250, 300, 350, and 400 Ω cm; thicker lines represent larger values). *E–H*: R_N as a function of R_i (50–400 Ω cm), with different curves representing different values of R_m (10, 15, 20, 25, 30, 35, 40, 45, 50, 55, and 60 kΩ cm^2; thicker lines denote larger values). Within the range of parameters explored, the relationship between R_N and either R_m or R_i is almost linear with slope < 1.

Both of these distributions overlapped the distribution of terminations in stratum radiatum. The latter distribution had the largest range of L values and evidenced two or more prominent peaks. The region of overlap between terminations in oriens and radiatum was responsible for the major peak on the left side of the overall distribution. Terminations in stratum lacunosum-moleculare are responsible for the peak on the right side of the overall distribution. Thus there is an obvious relationship between distribution of L and the laminar organization of the CA1 region of the hippocampus.

VOLTAGE TRANSFER TO THE SOMA. The electrotonic length of dendritic processes is conventionally evaluated from the steady-state transfer of voltage from the soma to the dendrites (*Eq. 5*). Accordingly, the results presented thus far were based on the steady-state voltage attenuation away from the soma (centrifugal transfer). However, one is often inter-

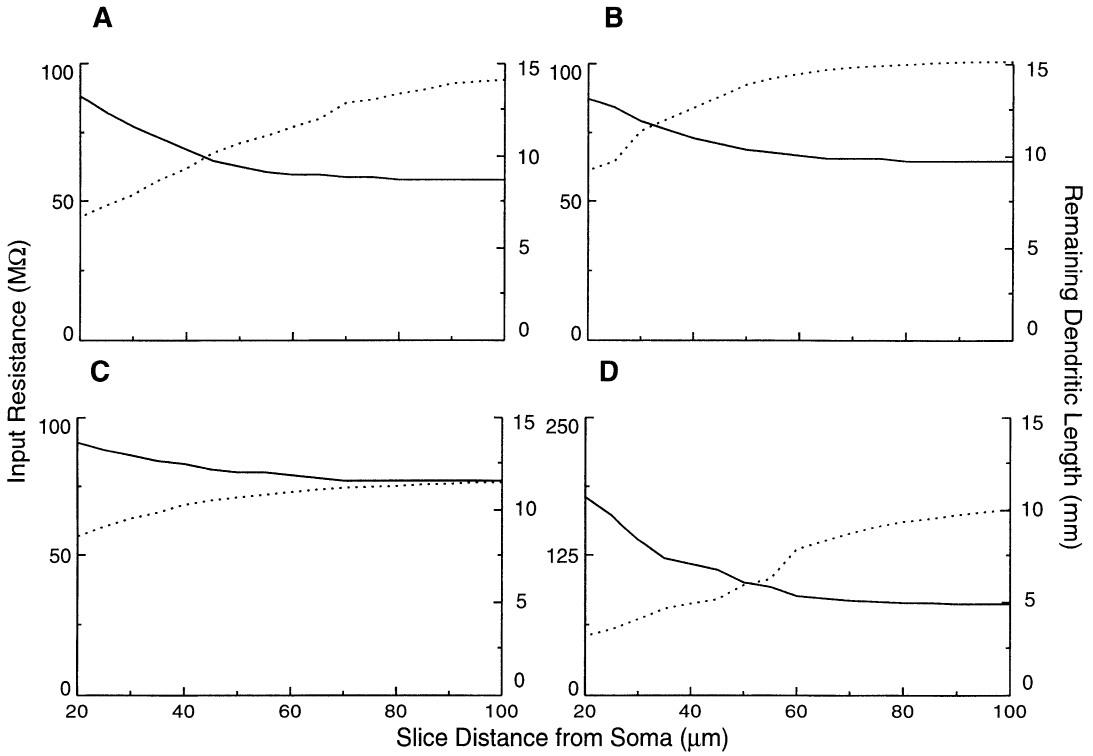

FIG. 5. R_N and physical dendritic length as a function of dendritic pruning. *A–D* correspond to the cells in Fig. 1. Pruning was done by passing a plane through the arbor to section the dendrites at various distances above the soma. The plane was parallel to the surface of the slice (perpendicular to the long axis of the hippocampus) and at various distances above the center of the soma. The resulting R_N (——; *left ordinate*) and remaining total dendritic lengths (· · ·; *right ordinate*) are plotted against the distance of the "cutting" plane from the soma.

ested in transfer of voltage in the opposite direction (centripetal transfer). It is well known that the transfer is not the same in the two directions (Brown et al. 1992; Carnevale and Johnston 1982; Rall and Rinzel 1973; Tsai et al. 1994b). Even when the equivalent cylinder model is appropriate for the centrifugal voltage transfer, it has limited applicability (described below) for understanding centripetal transfer (Jack et al. 1983; Tsai et al. 1994b).

To evaluate voltage transfer toward the soma we again used *Eq. 6,* which does not assume the equivalent cylinder model, but this time we based the calculation on the steady-state attenuation of voltage from the dendritic tips to the soma. These centripetal L values were larger, meaning that there is more voltage attenuation in this direction. The distributions of L values in all four cells are shown in Fig. 8, *A–D.* The L distributions again evidenced multiple peaks, a large CV, and a large range of values. Note that $L \geq 3.0$ for some processes, which means that, even in the steady state, less than $(1/e)^3 \approx 5\%$ of the voltage applied to some of the dendritic tips would reach the soma through passive spread. As we illustrate later, transient events are attenuated even more.

Again there was an evident relationship between the peaks in the overall distribution and the laminae in which the processes terminated. The L distributions for terminations in stratum oriens and radiatum overlapped and gave rise to the large peak on the left side of the overall distribution, whereas the L distribution of terminations in lacunosum-moleculare were responsible for the right side of the overall distribution. In regard to the relative locations of the three distributions, there was one principal difference between these results and those in Fig. 7; namely, in two of the cells (Fig. 8, *B* and *D*), some of the terminations in stratum radiatum were electrotonically closer to the soma than some of the terminations in stratum oriens.

These features of the L distribution are not specific to one set of values of R_m and R_i. The effects of varying R_m and R_i, respectively, are illustrated in Fig. 8, *E* and *F.* As R_m decreases (Fig. 8*E*) or R_i increases (Fig. 8*F*), the distribution of L shifts to the right and displays more peaks. Regardless of the values of the electrical constants, in all four cells the distribution was multimodal and there was a large range and CV.

These results suggest that the equivalent cylinder model does not adequately characterize the dendritic arbor of hippocampal CA1 neurons because different processes terminate at widely varying electrotonic distances from the soma.

Passive spread of somatic events to the dendrites

Up to this point we have been concerned only with steady-state attenuation and cell R_N, properties that are not affected by C_m. Next we extend the analysis to include transient events, in which C_m has a very significant role. The present section evaluates transients initiated in the soma and the following section examines transients initiated in the dendrites.

SOMATIC CURRENT STEP. We began by simulating the application of a current step (0.75 nA) to the soma of the neuron shown in Fig. 9*A* (*cell 822*), computing the time course

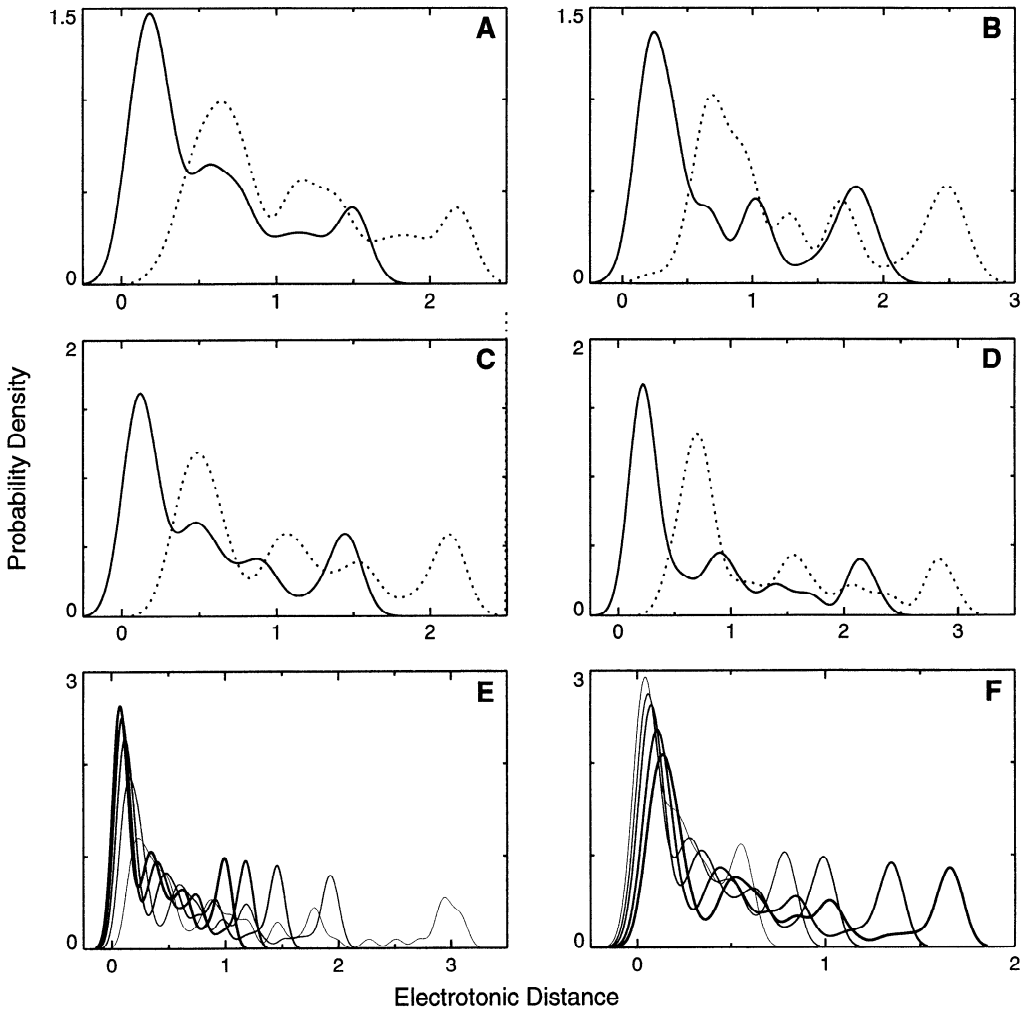

FIG. 6. Electrotonic distances of dendritic terminations for centrifugal voltage spread (soma to dendritic tips). *A–D*: comparison of distribution of electrotonic distance X computed with the use of *Eq. 5* (· · ·), which assumes the equivalent cylinder model, and the new electrotonic distance L from *Eq. 6* (——), which does not make this assumption. Both equations give multimodal distributions with large variances. L has somewhat lower mean and higher CV (see Table 5). R_m = 30kΩ cm^2, R_i = 200 Ω cm. *E*: distributions of L for *cell 822* (*C*) computed for 5 different values of R_m (10, 20, 30, 40, and 50 kΩ cm^2). Larger values of R_m correspond to thicker line widths. *F*: distributions of L for *cell 822* computed for 5 different values of R_i (100, 150, 200, 300, and 400 Ω cm), larger values corresponding to thicker line widths. Gaussian smoothing used σ = 0.1 (*A–D*) or 0.06 (*E–F*) electrotonic unit. In this and subsequent figures, dendrite diameters were corrected by 0.5 μm (see text).

of membrane potential at the soma and the four dendritic recording sites indicated by circles. It took ~100 ms for voltage to approach steady state at any of these sites (Fig. 9*B*). Steady-state voltage transferred to the basilar dendrites (stratum oriens) with little attenuation. Moving up the apical dendrites, the steady-state voltage attenuation progressively worsened. The voltage attenuation from the soma to the distal portion of stratum radiatum was >50%.

TABLE 5. *Electrotonic distance distributions*

	Cell				
	503	*602*	*822*	*913*	Average
$X_{tip} = \cosh^{-1}(V_{soma}/V_{tip})$					
Mean	0.97	1.38	1.07	1.42	1.21
Range	1.64	2.46	1.85	2.53	2.12
CV	0.52	0.52	0.58	0.57	0.55
$L_{tip} = ln(V_{tip}/V_{soma})$					
Mean	0.46	0.81	0.55	0.84	0.67
Range	1.20	1.98	1.44	2.20	1.71
CV	0.82	0.77	0.89	0.85	0.83

Based on corrected diameters—see text. CV, coefficient of variation.

Increasing R_m from 30 to 150 kΩ cm^2 improved steady-state voltage transfer but had little effect on the early transients (results not shown). After a somatic current step, substantial voltage gradients were present throughout the dendritic tree that were relatively unaffected by increasing R_m, even to an unrealistically high value. This is because the early part of any transient response depends on high-frequency components of the signal, which are preferentially shunted by the low impedance of C_m. However, the later part of the response involves low-frequency and steady-state components to which C_m presents a much higher impedance. Therefore changing R_m can alter steady-state attenuation substantially while having little effect on transient events.

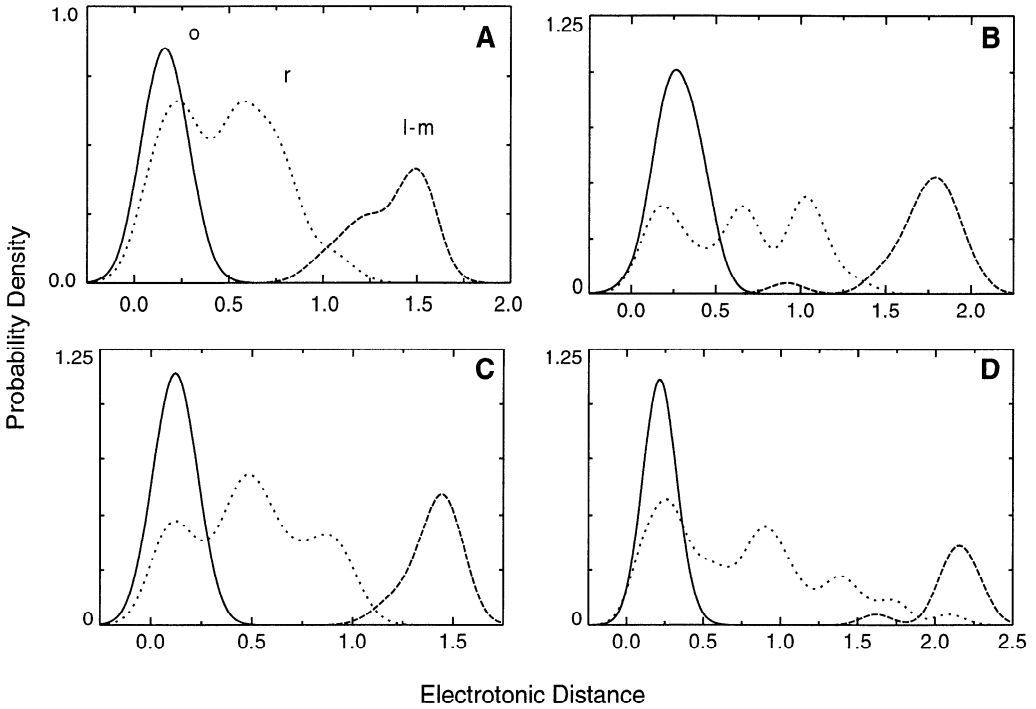

FIG. 7. Relationship of peaks in L distribution to laminae. A–D: centrifugal electrotonic distances from soma to dendritic tips were subdivided into 3 populations according to the anatomic layer in which the dendritic process terminated (stratum oriens, —— labeled "o"; stratum radiatum, · · · labeled "r"; stratum lacunosum-moleculare, – – – labeled "l-m"). In all 4 cells, the L distribution for stratum oriens (basilar dendrites) was unimodal and had the smallest mean. The L distribution for stratum lacunosum-moleculare was also unimodal but had a much larger mean. The distribution of L for stratum radiatum had the largest variation and was multimodal. Procedures and parameters were the same as those used in Fig. 6. Curves are normalized so that the total of the areas under the 3 subsets was unity. For Gaussian smoothing, $\sigma = 0.1$.

SOMATIC VOLTAGE STEP. Application of a voltage step to the soma also produced spatial gradients of voltage along the dendritic arbor (Fig. 9*C*). Again, steady-state voltage transfer was best to the basilar dendrites and worst to the distal apicals in the stratum lacunosum-moleculare. Voltage at the dendritic recording sites approached steady state in 10–70 ms depending on location. As with the response to a current step, increasing the value of R_m from 30 to 150 kΩ cm^2 improved steady-state transfer but had little effect on early transients (<15 ms following onset of the voltage step).

There are three differences and one striking similarity between the results obtained under current- and voltage-clamp conditions (compare Fig. 9, *B* and *C*). First, the voltage at the soma rose instantaneously for a voltage step but gradually for a current step. Second, the transient spatial gradients were steeper under voltage-clamp conditions. This is because the rate of change of potential in the soma was smaller after the current step. Third, the steady state was reached faster after a voltage step than a current step. However, neither current clamp nor voltage clamp at the soma could change dendritic membrane potential rapidly. The maximum speed with which an ideal voltage clamp can control the dendritic potential was very limited, even when R_m was high, because most of the initial transmembrane current is capacitive. These results show that hippocampal CA1 pyramidal neurons are far from isopotential for transient voltage commands and that the dendritic potential cannot be rapidly clamped to new values.

SOMATIC ACTION POTENTIAL. Up to now, we have examined only the kinds of inputs to the soma that an experimenter might impose under current- or voltage-clamp conditions. We were curious to examine naturally occurring transients, such as action potentials, under conditions in which the dendrites remain passive. With modified Hodgkin-Huxley conductances introduced into the soma of the otherwise passive model, a train of somatic spikes was triggered by a depolarizing current pulse (Fig. 9*D*). Compared with the response to a somatic current or voltage step, the attenuation was much more profound in all four recording sites, although the rank orders remained the same. The largest response was in the basilar dendrites, where the amount of depolarization per action potential was reduced to a few millivolts. The smallest response was in the distal stratum lacunosum-moleculare, where the spike train produced only a barely detectable ripple riding on a slow and very slight depolarization.

Passive spread of dendritic events to the soma

Thus far we have considered only transfer away from the soma. In studies of synaptic physiology, however, one is often most interested in transfer from the dendrites to the soma. Here we present responses in the soma to synaptic inputs on different parts of the dendritic tree. Even if the equivalent cylinder model had been appropriate for analyzing the spread of voltage from the soma to the dendrites, it would not have been appropriate for the present analysis.

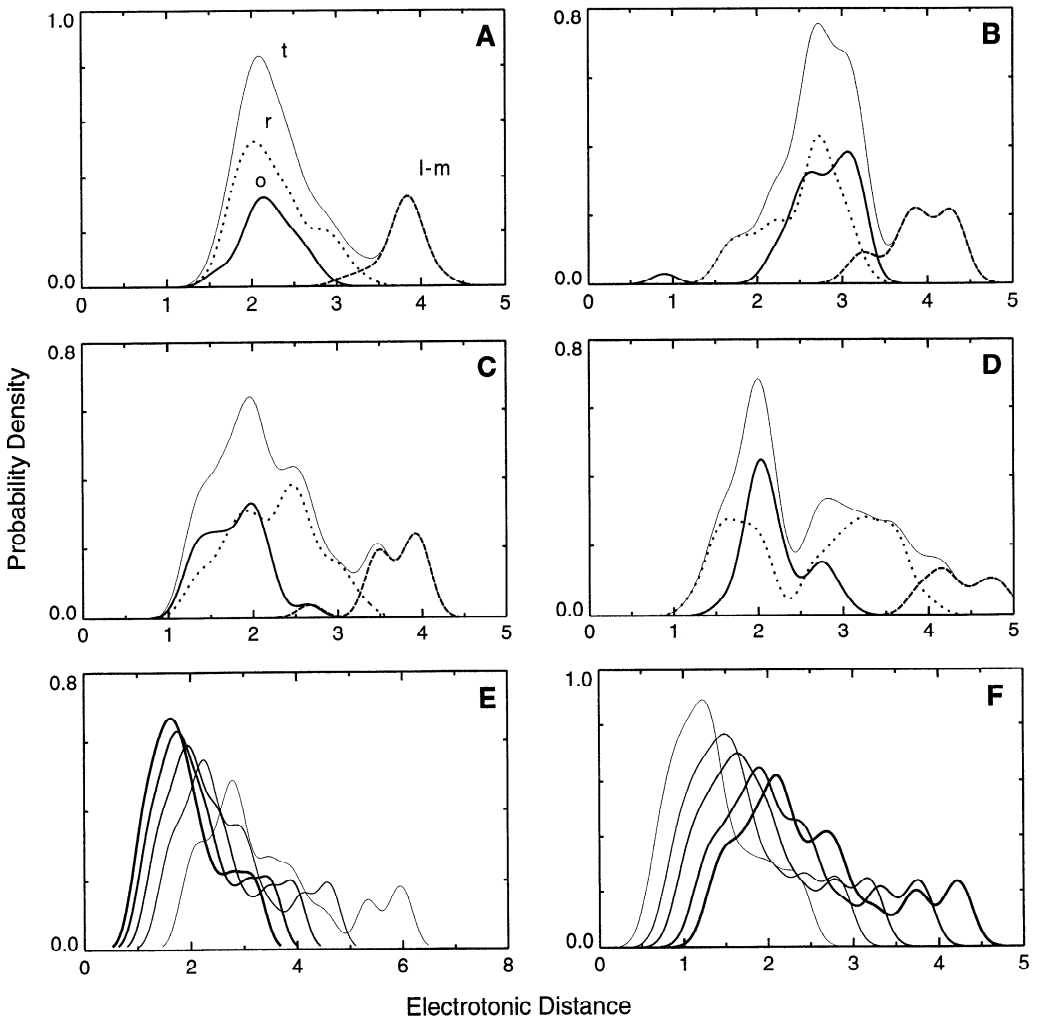

FIG. 8. Distribution of L for centripetal voltage spread (from branch tips toward the soma). A–D: electronic distances were calculated with the use of *Eq. 6*. With the use of the compartmental model, current sources were placed successively at each dendritic tip and the resulting steady-state voltages were measured locally and at the soma. Total distribution (thin line labeled "t") and distributions separated according to anatomic layer (stratum oriens, —— labeled "o"; stratum radiatum, · · · labeled "r"; stratum lacunosum-moleculare, – – – labeled "l-m") are shown. The distributions follow a similar pattern to that of distributions for transfer of voltage from the soma, but with a larger mean. They were qualitatively unaltered by variations in R_i or R_m. E: centripetal L distributions are shown for 5 values of R_m (10, 20, 30, 40, and 50 kΩ cm^2 in *cell 822* (*C*), where increasing line thickness denotes increasing values of R_m). F: distributions are shown for 5 values of R_i (100, 150, 200, 300, and 400 Ω cm in *cell 822* (*C*), where increasing line thickness denotes increasing R_i). Except where noted, procedures and parameters were the same as in Fig. 6. For Gaussian smoothing, $\sigma = 0.1$.

The reason is that the equivalent cylinder model requires the additional assumption—which is not characteristic of most neurophysiological studies—that all of the dendritic processes at a given electrotonic distance from the soma simultaneously receive the same synaptic input.

SPREAD OF SYNAPTIC POTENTIALS. We first examined the spread of synaptic potentials. In successive simulations, synapses were activated at four different locations (see Fig. 9*A*) on the dendritic tree (Fig. 10). Regardless of the location, there was enormous attenuation of the peak response measured at the soma (<0.2 mV vs. 5–6 mV at the synaptic site). The time to peak in the spine head was <5 ms and changed very little with location. The somatic time to peak was always slower and was dependent on the synaptic location (Table 6). Delay and attenuation increased dramatically as the electrotonic distance from the synapse to the soma (*Eq. 6*) increased. Depending on the location and electrical constants, the delay in time to peak ranged from <5 ms (basilar dendritic site, R_i = 100 Ω cm; Table 6*C*) to >40 ms (distal apical site, R_m = 60 kΩ cm^2; Table 6*B*).

SPREAD OF SYNAPTIC CURRENT. A similar analysis was performed on the peak synaptic current. In these experiments the synapses were successively activated at the same four locations on the dendritic tree. The current peaks measured by an ideal voltage clamp at the soma were much smaller than the actual synaptic currents at the subsynaptic membrane (Fig. 11*B*). At the synaptic site, the peak currents were ~27 pA, but the peaks measured at the soma were only in the range of 0.5–9 pA. At all four locations the time to peak of current in the spine head was ~0.6 ms and was relatively location independent. The somatic time to peak was always slower and depended strongly on synaptic location.

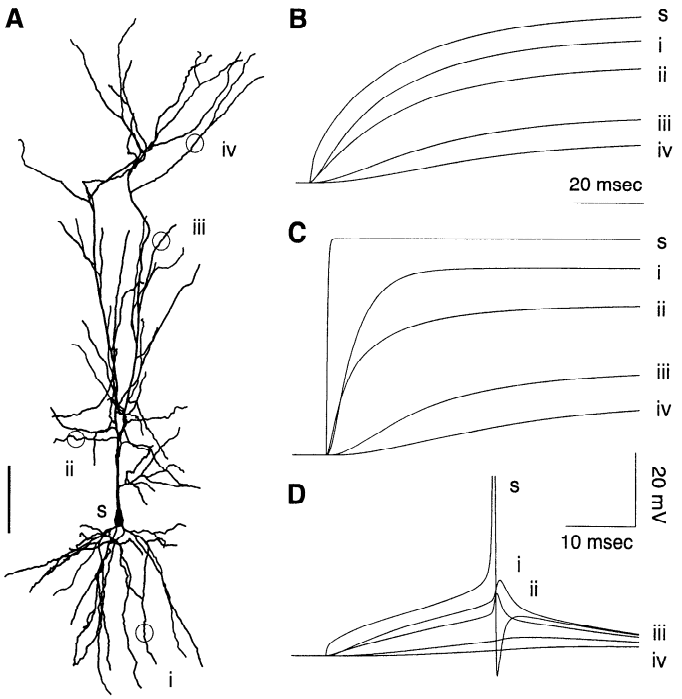

FIG. 9. Effects of somatic events on dendritic membrane potential. In these simulations, $R_m = 30\ k\Omega\ cm^2$, $R_i = 200\ \Omega$ cm. *A*: anatomic reconstruction of hippocampal CA1 pyramidal neuron [Fig. 1*C* (*cell 822*)]. Dendritic locations i–iv are 224, 194, 433, and 639 μm from the soma s, respectively. *B*: response to a current step of 0.75 nA injected at the soma beginning at $t = 5$ ms. *C*: somatic membrane potential was stepped from rest (−60 mV) to 0 mV at $t = 5$ ms with the use of a simulated voltage clamp. *D*: voltage-dependent channels (Hodgkin-Huxley type I_{Na} and I_K; see METHODS) were added to the soma only. Repetitive spiking was induced by injecting 0.25 nA from $t = 5$ ms at the soma. Distance scale in *A* is 100 μm; time scale is 20 ms for *B*, 10 ms for *C* and *D*.

It is important to note that application of a somatic voltage clamp at the resting potential (−60 mV) had practically no effect on the synaptic potential amplitude at the subsynaptic membrane (Fig. 10*B*). At the more proximal sites, the somatic clamp slightly accelerated the decay of potential at the subsynaptic membrane. Clamping the soma more negatively, to −100 mV (Fig. 11*A*), did reduce the peak depolarization at synaptic sites, but this effect resulted from the more negative initial steady-state potential at these sites rather than a reduction in the voltage excursion. Because a perfect space clamp implies uniform control of the membrane potential throughout the dendritic tree, the results presented thus far make it clear that one cannot hope to achieve a perfect space clamp in rat CA1 pyramidal neurons. This is an inescapable consequence of the electrotonic architecture of these cells, and it must be considered in the design and interpretation of any experiment in which control of membrane potential (V_m) at nonsomatic locations is essential (see DISCUSSION).

Comparison of cable effects on different measures of synaptic response

The results described above indicate that synaptic signals originating in many dendritic locations can undergo extreme attenuation and distortion as they passively spread toward the soma. We quantified dendritic attenuation in terms of the "fractional response" (f), defined as the ratio of the peak somatic response to the peak response in the subsynaptic membrane. The values of f were examined as a function of the dendritic location and the assumed electrical parameters.

Table 6 summarizes these effects for several combinations of R_m and R_i values and as a function of the location of the synapse on the dendritic tree and the quantity measured. At all four dendritic sites, and within a reasonable range of parameter values, the peak somatic voltage response was at most a few percent of the value at the subsynaptic membrane. The maximum slope of the rising phase of the excitatory postsynaptic potential, a measure sometimes used to avoid contamination from later events, suffered even greater attenuation than the peak voltage. Response measurements based on peak current, on the other hand, evidenced less attenuation than did peak voltage. Charge, which is the integral of current, attenuates much less than voltage and slightly less than peak current.

Regardless of the synaptic location, the severity of attenuation was (in increasing order): charge, peak current, peak

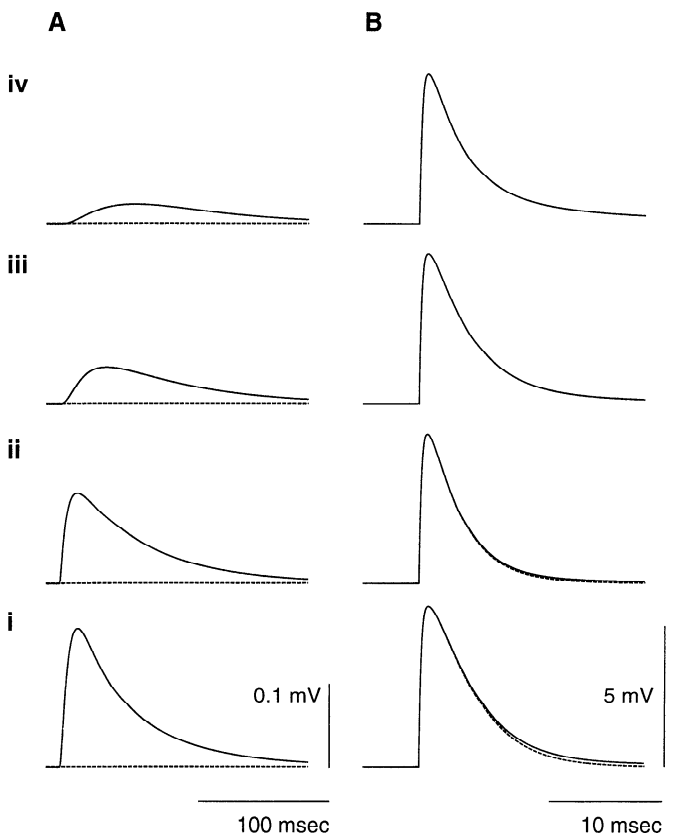

FIG. 10. Voltage transients during current and voltage clamp of synaptic events (same cell as in Fig. 9). A synaptic conductance was activated at 1 of 4 sites during current- or voltage-clamp recordings at the soma. The sites correspond to the locations illustrated in Fig. 9*A* (i: basilar dendrites; ii: proximal apical dendrites; iii: medial apical dendrites; iv: distal apical dendrites). The synaptic conductance had a time to peak of 0.55 ms, a decay time constant of 2.5 ms, and a peak conductance of 0.5 nS (see METHODS). *A*: voltage at soma during simulated voltage clamp to resting potential (– – –) and during current clamp (——). *B*: subsynaptic voltage as recorded at the spine head for 4 different locations during voltage clamp (– – –) or current clamp (——). The voltage- and current-clamp traces nearly superimpose in all 4 cases, indicating that even an ideal somatic voltage clamp almost completely fails to control the subsynaptic potential. In these simulations, $R_m = 30\ k\Omega\ cm^2$, $R_i = 200\ \Omega$ cm.

TABLE 6. *Synaptic response measurements*

Location	Fractional Response				Delay, ms	
	Q_{total}	I_{peak}	V_{peak}	V_{slope}	I_{peak}	V_{peak}
	A. R_m = 30 kΩ cm^2; R_i = 200 Ω cm; R_N = 63 MΩ					
i	0.104	0.0245	0.00426	0.000104	14.6	27.9
ii	0.258	0.0593	0.00796	0.000322	8.5	17.1
iii	0.639	0.241	0.0203	0.00225	2.2	6.1
iv	0.864	0.341	0.0286	0.00292	3.0	6.2
	B. R_m = 60 kΩ cm^2; R_i = 200 Ω cm; R_N = 106 MΩ					
i	0.124	0.0308	0.00715	0.000122	17.3	40.2
ii	0.298	0.0666	0.0107	0.00034	9.2	23.2
iii	0.683	0.247	0.0221	0.00219	2.3	7.3
iv	0.919	0.352	0.0312	0.00294	3.0	7.0
	C. R_m = 30 kΩ cm^2; R_i = 100 Ω cm; R_N = 53 MΩ					
i	0.263	0.0576	0.0127	0.000442	10.2	21.4
ii	0.438	0.114	0.0184	0.00107	5.7	13.2
iii	0.752	0.336	0.0361	0.00408	1.6	6.0
iv	0.933	0.493	0.0463	0.00751	1.9	4.9

Cell 822, based on corrected diameters—see text. I_{peak}, peak current; V_{peak}, peak voltage; V_{slope}, voltage slope; R_N, input resistance; for other abbreviations, see Table 2.

voltage, and voltage slope. For all quantities, the attenuation was less as R_m increased, but the effect was smaller than might have been expected, the primary loss of current being capacitative. The attenuation was also less for all quantities as R_i decreased. With respect to distortion of the time course of the synaptic event, the delay in time to peak was greater for peak voltage than for peak current. For both measures, the delay increased as R_m increased and decreased as R_i decreased.

DISTRIBUTION OF SYNAPTIC RESPONSES. These conclusions were not specific to the four synaptic sites chosen thus far. Earlier, we used the relative frequency distribution of electrotonic distances of the dendritic terminals to characterize the electrical structure of the entire dendritic tree. Here, we used an analogous approach to characterize the attenuation of signals of synaptic origin over the entire dendritic arbor to the soma (Fig. 12). To do this, individual synapses were activated in separate simulations as described above. For each dendritic compartment, one synapse was activated under current clamp and then voltage clamp, and measurements of voltage and current at the soma were made as for Table 6. The contribution of a measurement at any particular compartment to the overall distribution for that measurement was proportional to the length of the compartment. Assuming that the density of synapses per unit length of dendrite is uniform, this procedure gives a probability density that weights the contribution of synapses at different electrotonic distances from the soma.

Figure 12 shows the probability distributions of peak current [Fig. 12*A*, I_{peak} (pA)], charge [Fig. 12*B*, Q (fC)], time to peak current [Fig. 12*C*, $I_{t\text{-}peak}$ (ms)], peak voltage [Fig. 12*D*, V_{peak} (mV)], voltage slope [Fig. 12*E*, V_{slope} (V/s)], and time to voltage peak [Fig. 12*F*, $V_{t\text{-}peak}$ (ms)], plotted for three different laminae (· · ·, stratum radiatum; thick ——, stratum oriens; – – –, stratum lacunosum-moleculare; thin ——, total). Note that Gaussian filtering caused the probability density to be slightly >0 at values just to the left of the origin on the abscissa. All these distributions showed high variance and multiple modes corresponding to the anatomic laminae. This effect was very pronounced in the measurements that suffer the least attenuation (particularly charge) but less evident in the measurements that undergo the most attenuation (particularly voltage slope).

DISCUSSION

In this study we used computer simulations to assess the electrotonic structure of anatomically reconstructed pyramidal neurons from the CA1 region of the hippocampus. We have focused especially on questions of interest to the practicing hippocampal physiologist, whose concern with electrotonus stems from the fact that it limits how well membrane potential can be controlled from the soma and determines how much the dendrites attenuate and prolong the observed waveforms produced by synaptic inputs. The electrotonic architecture of a cell is also important in theoretical studies of biological information processing because it shapes the cellular response to distributed synaptic inputs and determines the manner in which Hebbian synapses self-organize (Brown et al. 1988a, 1991a,b, 1992; Fisher et al. 1993; Kairiss et al. 1992; Mainen et al. 1990; Tsai et al. 1994a).

Dendritic electrotonus and active membrane

Before considering the implications of our results, it is appropriate to consider the effects of active channels on electrical signaling in dendrites. Magee and Johnston (1995) showed that depolarizations of a few millivolts could activate sodium and calcium conductances in the apical dendrites of CA1 pyramidal neurons, so these conductances might contribute to neuronal "small-signal" properties. As pointed out in METHODS, the parameters we used in our models are

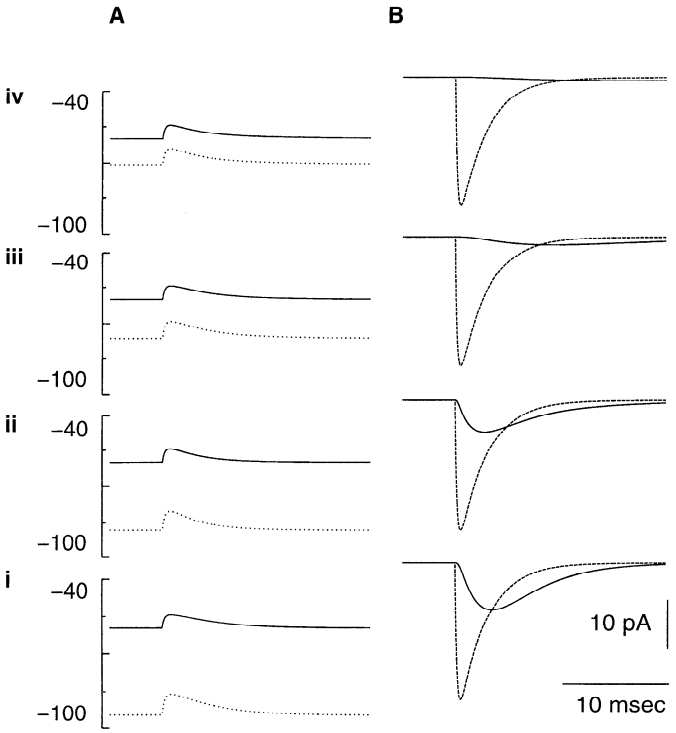

FIG. 11. Current transients during voltage clamp of synaptic events (same cell as in Fig. 9). A synaptic conductance was activated on a spine located at 1 of 4 sites of the dendritic tree as in Fig. 10. *A*: soma was held by voltage clamp to −60 and −100 mV. The membrane potential at the synapse during these 2 conditions is shown. The baseline membrane potential achieved by the step to −100 mV is closer to the applied clamp voltage in the more proximal groups of synapses (i, ii; cf. Fig. 9), reducing the peak potential during synaptic activation. However, voltage control of the transient potential during synaptic activation is poor regardless of holding potential or synaptic location. Therefore the voltage change at the postsynaptic site during synaptic activation is little affected by these differences. *B*: comparison of measured synaptic current during clamp to rest, (−60 mV; ——) and actual synaptic current (· · ·). There is significant attenuation of measured peak synaptic current and distortion (slowing) of the waveform of the response, and these effects increase with distance (i–iv). Despite lack of voltage control, the somatic clamp captures a large fraction of the total synaptic charge (see Table 6).

based on experimental measurements that would automatically have included the small-signal effects of active channels. These parameters reflect the net contributions from passive and active membrane currents over the range in which total membrane current is a relatively linear function of membrane potential. Although the resulting linear models do not represent the entirety of neuronal electrical signaling, they describe the basic scaffolding within which any other currents generated by active processes must operate. Such models are useful for assessing the experimental accessibility of currents and voltages produced by synaptic and active channels to microelectrode measurements; furthermore, the predictions they generate about the efficacy of remote synaptic inputs lead to inferences about the function of active channels in synaptic integration.

The extent to which active channels participate in electrical signaling is an empirical issue that remains to be resolved, and relatively little is known about their actual role in CA1 pyramidal neurons. There is some evidence from neocortical pyramidal neurons, where it appears that dendritic persistent sodium current can enhance synaptic currents (Schwindt and Crill 1995). However, other experiments indicate that dendritic electrotonus per se may be quite linear even for depolarizations as much as 50 mV from rest (Stuart and Sakmann 1995). Although somatic depolarizations >5 mV could activate an inward current in the soma and axon, this generally did not make a substantial contribution to the net depolarization unless the transient was >10 mV (Stuart and Sakmann 1995).

These observations suggest that, even though the typical fluctuations of membrane potential that occur spontaneously or that are evoked by activation of one or even several synaptic inputs may activate voltage-dependent channels, these fluctuations may not be large enough to bring out a net nonlinearity. Furthermore, the source of the nonlinearity may be localized to the soma and axon, which means that it would affect only the centripetal spread of voltage transients, and not centrifugal voltage propagation. Therefore attenuations and electrotonic distances calculated for voltage spreading away from the soma would be unaltered. Although attenuations and distances in the opposite direction would be smaller than those we calculated, the effect would be minimal for signals with amplitudes of <5–10 mV. Thus linear electrotonic analysis may provide a good description of electrical signaling in neurons that is useful over a wide operating range.

Equivalent cylinder representation fails to capture electrotonic structure

Our primary aim in initiating this project was to analyze the electrotonic architecture of hippocampal CA1 pyramidal neurons on the basis of the best available anatomic and biophysical data. In performing this analysis we were compelled to reexamine the rationale and applicability of the equivalent cylinder model of dendritic electrotonus, which has enjoyed extensive historical usage, is completely specified by just a few parameters, and has analytical solutions for certain responses to particular types of inputs (Butz and Cowan 1974; Holmes and Rall 1992a,b; Jack et al. 1983; Rall 1977). Although this classical approach has an appealing simplicity, empirical observations force the conclusion that the assumptions it requires do not apply to CA1 pyramidal neurons. Furthermore, it does not capture useful biological information regarding passive electrical signaling in CA1 pyramidal neurons.

For a dendritic tree to be reducible to an equivalent cylinder, it must satisfy two primary stipulations: that all terminations be electrically equidistant from the soma, and that the 3/2 power rule hold at each branchpoint. Neither of these assumptions held for the four cells we studied. Even in the simplest case of steady-state transfer of voltage from the soma to the dendrites, the distributions of electrotonic lengths (Figs. 6 and 8) and branchpoint diameters (Fig. 3) deviated severely from the assumptions of the model. The large variance of electrotonic lengths indicates that the electrotonic structure of CA1 pyramidal neurons is not well characterized by a single measure.

The disparity between theoretical requirements and experimental observations was not subtle; nor did it seem likely to result from simple biological variability. The dramatic failure to meet the requirements of the equivalent cylinder

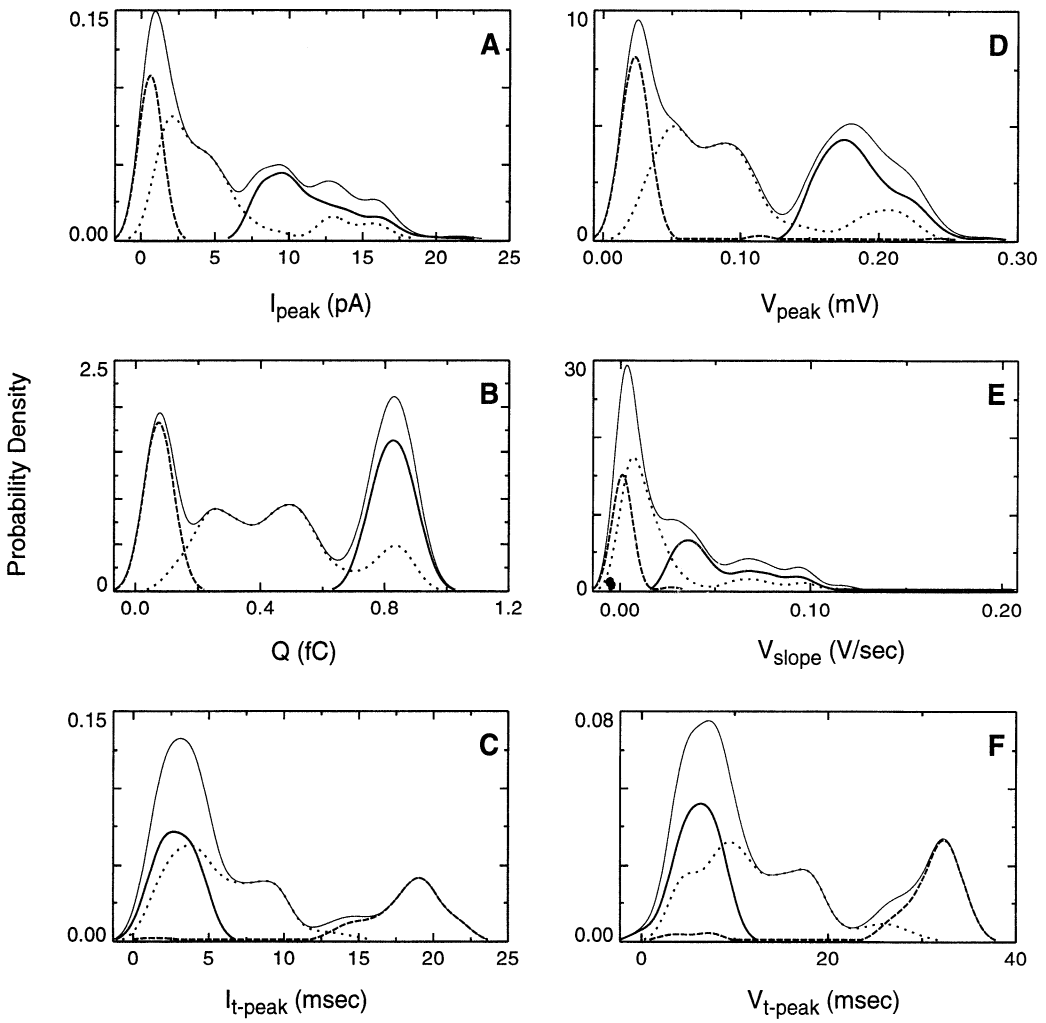

FIG. 12. Theoretical distributions of synaptic measurements (same cell as in Fig. 9). Probability distributions for several synaptic measurements were obtained by simulating a large number of synaptic events occurring in individual simulations on spines distributed uniformly through the dendritic arbor. This was done by simulating 1 spine per dendritic compartment and scaling the measurements by the compartment area. Each synaptic conductance had a time to peak of 0.55 ms, a decay time constant of 2.5 ms, and a peak conductance of 0.5 nS (see METHODS). The distributions are separated by anatomic layer (stratum oriens, heavy ——; stratum radiatum, · · ·; stratum lacunosum-moleculare, – – –; total, thin ——). *A–C*: measurements were made by simulated somatic voltage clamp. *A*: peak synaptic current (pA). *B*: synaptic charge (fC). *C*: time to peak synaptic current. *D–F*: measurements were made at the soma under current clamp conditions. *D*: peak synaptic potential (mV). *E*: initial slope of synaptic potential (V/s, calculated between 1 and 25% of peak value). *F*: time to peak synaptic potential. In all cases, histograms were smoothed with a Gaussian kernel with σ of 5% the SD of the entire distribution (all 3 laminae) and normalized to have unit area under the entire distribution.

representation was qualitatively unaffected by a diameter correction of 0.5 μm or by varying R_i or R_m over a wide range. Furthermore, there was nothing unusual about the particular CA1 neurons we studied, which were selected according to stringent criteria for completeness of fill and which had quantitative morphometry that was similar to previous reports (Amaral et al. 1990; Ishizuka et al. 1995).

This failure of the equivalent cylinder representation does not appear to be unique to CA1 pyramidal cells. Morphometric analyses of many other neuronal classes suggest wholesale violation of the 3/2 power rule (Desmond and Levy 1984; Hillman 1979; Korogod et al. 1994; Ulrich et al. 1994). Likewise, computed centrifugal voltage attenuations are far from identical at all dendritic terminations in other cell classes (Korogod et al. 1994; Major et al. 1994; Turner 1984; Ulrich et al. 1994).

Ignoring for a moment the fact that the conditions required by the equivalent cylinder model are not satisfied by neurons analyzed by ourselves or others, one might yet ask whether there is some way in which this approach could have some utility. If the goal is limited to simulating the charging curve of a cell in response to a current or voltage step applied at the soma, the answer is "yes," with the qualification that experimentally observed multiexponential decays are notoriously easy to approximate to a high degree of apparent accuracy by sums of a few exponential terms that individually have grossly inaccurate amplitudes and time courses (Aubard et al. 1987; Yeramian and Claverie 1987). Because of this fact, estimates of electrotonic architecture that are based on charging curves can be uncertain even under the best of circumstances.

Even so, in the past when detailed quantitative morphometry was unobtainable, equivalent cylinder approximations at

least offered a method for qualitatively describing the electrical properties of a cell as seen from the soma. At the same time, this independence from anatomy is actually the greatest weakness of the ball-and-stick approach, making it essentially a curve-fitting procedure that tunes a highly abstract model to mimic experimentally observed charging curves. For many if not most important questions about electrical signaling in neurons, this level of abstraction is too removed from the biology to be relevant or useful, and it can actually be misleading.

It should be noted that our new definition of electrotonic distance L (*Eq. 6*) recognizes the fact that voltage attenuation is direction dependent, regardless of whether the cell has an equivalent cylinder representation (Rall and Rinzel 1973) or not (Carnevale and Johnston 1982). Thus each point in the cell has two electrotonic distances from the soma, one for centrifugal and the other for centripetal voltage spread. This is amply borne out by comparison of centrifugal and centripetal voltage attenuations and electrotonic distances (e.g., Fig. 6 vs. Fig. 8). These observations underscore the need to know the efficacy of signal transfer in two directions along each branch in order to have a complete understanding of electrical signaling in any neuron with nontrivial electrotonic extent.

However, the classical electrotonic distance X is defined solely in terms of voltage propagating away from the soma. Thus *Eq. 5* does not apply to voltage spreading toward the soma, even though the centripetal direction is clearly important to neuronal function and the interpretation of experimental observations. There is no expression equivalent to *Eq. 6* that would relate classical electrotonic distance X to the attenuation of voltage spreading from some point in the cell to the soma.

Electrotonic distribution of dendritic terminations is laminated

By all measures, dendritic terminations were located at widely varying electrotonic distances, both for voltage propagating away from [X (*Eq. 5*) and centrifugal L (*Eq. 6*)] or toward (centripetal L) the soma. In each cell, the frequency distribution of these distances was not centered around a single peak; instead it was characterized by large variance and multiple peaks (Figs. 6 and 8). Furthermore, the overall form of this multimodal distribution was independent of the particular values assumed for the electrical properties of membrane and cytoplasm. The robustness of this finding suggests some underlying cause other than "biological variability." Subsequent analysis suggested that the distribution of terminations reflects the laminar distribution of major afferent projections to CA1 cells (Figs. 7, 8, and 12) (Mainen et al. 1991).

Sensitivity of computed R_N to anatomic and biophysical parameters

For these CA1 pyramidal neurons from rat hippocampus, R_N computed from the uncorrected anatomic data averaged ~2.3 times smaller than reported experimental observations under nystatin patch clamp in guinea pig CA1 pyramidal cells (Spruston and Johnston 1992). As we noted above, aside from species differences there are at least three possible reasons for this.

The calculated R_N would be too small if the computations employ too low a value for R_i. However, uncertainty about the true value of R_i does not by itself appear sufficient to account for a discrepancy of this magnitude.

A second factor to consider is overestimation of neurite diameters, a potential pitfall of morphometric systems that use conventional light microscopy (O'Boyle et al. 1993). The proportional effect of this error will be greatest on the membrane and cross-sectional areas of the thinnest dendritic branches, causing a substantial reduction of axial resistance and increase of membrane load. In electrotonically compact neurons such as CA1 pyramidal cells, even anatomically distal branches of the apical dendritic tree drain away a substantial fraction of the current that is injected at the soma, so diameter measurement errors could have large effects on computed R_N.

Finally, patch-clamp experiments tend to select for cells that lie close to the surface of the slice, which raises the possibility that biophysical measurements without anatomic confirmation will include cells that have suffered pruning of part of the dendritic tree. This should yield cells with artificially high R_N values, a prediction that was borne out by "simulated pruning" (Fig. 5). Because our anatomic data were from cells that tended to lie near the center of the slice, and pruned or incompletely filled cells were rejected, our models would not suffer from spurious overestimates of R_N.

Over the parameter ranges that we explored, R_m had a greater effect on the computed R_N than did R_i (Fig. 4).

Transient signals attenuate rapidly with distance

Current steps applied at the soma generated large potential gradients that relaxed slowly and incompletely with time (Fig. 9*B*). An ideal voltage clamp at the soma that produced an instantaneous step increase of somatic V_m decreased the charging time in the remainder of the cell only from ~100 to ~50 ms, and had no effect on the persistent spatial potential gradient (Fig. 9*C*). Increasing R_m reduced the DC potential gradient, but had little effect on the initial time course of charging whether under current clamp or voltage clamp, because C_m dominates membrane impedance at frequencies greater than $1/2\pi R_m C_m$ (less than ~5 Hz in these cells). Therefore early charging dynamics are regulated by C_m and R_i and are relatively independent of R_m. Furthermore, increasing R_m or R_i prolongs the somatically recorded time course of synaptic events (Table 6). Similar conclusions were reached by Spruston et al. (1993, 1994) in their study of space-clamp errors in cylindrical cable models and a model hippocampal CA3 pyramidal neuron.

This low-pass filtering explains the striking attenuation and delay of brief transients such as spikes spreading passively from the soma into the dendrites (Fig. 9*D*), or synaptic potentials or currents propagating from the dendrites to the soma (Figs. 10 and 11). It accounts for the fact that the peak amplitude of a brief transient suffers much more attenuation than does its integral (Table 6). The results in Table 6 suggest that charge provides the best measure and voltage the worst measure of the magnitude of the synaptic response, and that current reflects the time course more accurately than does voltage.

The distorting effects of electrotonic filtering on the time course of synaptic events observed at the soma are underscored by Fig. 12. This figure shows that the anatomic lamination of afferent pathways is reflected in the distributions of measured amplitudes, areas, and slopes. It should be noted that of all these measurements, the maximum slope of the somatically recorded postsynaptic potential (V_{slope}) was severely attenuated for most synaptic input sites. This indicates that, except for inputs that are physically very close to the recording site, V_{slope} is not a satisfactory indicator of the magnitude of synaptic events.

The severe attenuation of somatic action potentials spreading passively into the dendritic tree is clearly important to mechanisms of synaptic plasticity that are dependent on local membrane potential (Brown et al. 1988a,b, 1991a,b, 1992). In light of this, experimental observations that spikes can backfire into dendrites (Häusser et al. 1995; Jaffe et al. 1992; Spruston et al. 1995; Stuart and Sakmann 1994) take on a special significance.

Space clamp of transient signals is poor

Finally, and perhaps of greatest importance to the experimentalist, low-pass filtering imposes severe limitations on the ability of a somatic voltage clamp to impose or prevent V_m transients throughout the dendritic tree. These limitations can even affect regions where the steady-state potential follows the soma closely, such as the basilar dendrites or the proximal apical dendrite. As a consequence, over most of the dendritic tree a somatic voltage clamp did not significantly reduce the local amplitude of synaptically induced voltage transients in comparison with what would have occurred under current-clamp conditions (Figs. 10 and 11). Such escape of membrane potential in the subsynaptic region has been reported in an equivalent cylinder model of electrotonus in CA3 pyramidal neurons (Spruston et al. 1993).

This poor space clamp performance is a point of wide-reaching importance and may account for some of the disparate results that have appeared in the literature. For example, pairing the postsynaptic injection of depolarizing currents with presynaptic stimulation of the Schaffer collaterals has been observed to enable the induction of long-term potentiation in CA1 pyramidal neurons of rat (Kelso et al. 1986) and guinea pig (Wigstrom et al. 1986). However, hyperpolarization has been reported to block long-term synaptic potentiation induction in the rat (Malinow and Miller 1986) but not in the guinea pig (Wigstrom et al. 1982), which would seem to cast doubt on the dependence of long-term synaptic potentiation induction at this synapse on the membrane potential of the postsynaptic cell. As the results we present here indicate, this apparent contradiction could easily be caused by escape of the membrane potential in the subsynaptic region from the influence of somatic hyperpolarization. This might be due to a combination of interspecies differences in electrotonic architecture between rats and guinea pigs and differences in experimental procedures. It is noteworthy that Malinow and Miller took special care to maximize the effect of somatic potential on the subsynaptic region by attempting to stimulate fibers that would activate proximal synapses, using a large hyperpolarizing current (3 nA instead of 1 nA), and stimulating at a lower frequency than Wigstrom et al. (1982) (30 Hz rather than 50–100 Hz) in order to reduce the tendency of synaptic drive to override the effect of postsynaptic hyperpolarization on local membrane potential. Similar considerations about poor space clamp also apply to numerous other studies in which the logic of the experiment requires that the subsynaptic membrane potential be clamped to a fixed and known voltage (cf. Brown and Johnston 1983; Jaffe and Brown 1994; Johnston and Brown 1983; Jonas et al. 1993; Silver et al. 1992; Spruston et al. 1993; Stern et al. 1992).

We thank M. O'Boyle and R. Reyes for assistance with the three-dimensional reconstructions.

This work was supported by the Office of Naval Research, *DARPA,* the National Institute on Aging, and the Yale Neuroengineering and Neuroscience Center. Z. F. Mainen is a Howard Hughes Medical Institute predoctoral fellow.

Present addresses: Z. F. Mainen, Cold Spring Harbor Laboratory, Cold Spring Harbor, NY 11724. A. M. Zador, Salk Institute, 10010 N. Torrey Pines Rd., La Jolla, CA 92037.

Address for reprint requests: T. H. Brown, Dept. of Psychology, Yale University, P.O. Box 208205, New Haven, CT 06520-8205.

Received 28 August 1995; accepted in final form 30 April 1996.

REFERENCES

AMARAL, D. G., ISHIZUKA, N., AND CLAIBORNE, B. J. Neurons, numbers and the hippocampal network. *Prog. Brain Res.* 83: 1–11, 1990.

AUBARD, J., LEVOIR, P., DENIS, A., AND CLAVERIE, P. Direct analysis of chemical relaxation signals by a method based on the combination of Laplace transform and Padé approximants. *Comput. Chem.* 11: 163–178, 1987.

BARRIONUEVO, G. AND BROWN, T. H. Associative long-term potentiation in hippocampal slices. *Proc. Natl. Acad. Sci. USA* 80: 7347–7351, 1983.

BARRIONUEVO, G., KELSO, S. R., JOHNSTON, D., AND BROWN, T. H. Conductance mechanism responsible for long-term potentiation in monosynaptic and isolated excitatory synaptic inputs to hippocampus. *J. Neurophysiol.* 55: 540–550, 1986.

BEKKERS, J. M. AND STEVENS, C. F. Presynaptic mechanism for long-term potentiation in the hippocampus. *Nature Lond.* 346: 724–729, 1990.

BROWN, T. H., CHANG, V. C., GANONG, A. H., KEENAN, C. L., AND KELSO, S. R. Biophysical properties of dendrites and spines that may control the induction and expression of long-term synaptic potentiation. In: *Long-Term Potentiation: From Biophysics to Behavior,* edited by S. A. Deadwyler and P. W. Landfield. New York: Liss, 1988a, p. 201–264.

BROWN, T. H., CHAPMAN, P. F., KAIRISS, E. W., AND KEENAN, C. L. Long-term synaptic potentiation. *Science Wash. DC* 242: 724–728, 1988b.

BROWN, T. H., FRICKE, R. A., AND PERKEL, D. H. Passive electrical constants in three classes of hippocampal neurons. *J. Neurophysiol.* 46: 812–827, 1981.

BROWN, T. H. AND JOHNSTON, D. Voltage-clamp analysis of mossy fiber synaptic input to hippocampal neurons. *J. Neurophysiol.* 50: 487–507, 1983.

BROWN, T. H., MAINEN, Z. F., ZADOR, A. M., AND CLAIBORNE, B. J. Self-organization of Hebbian synapses in hippocampal neurons. In: *Advances in Neural Information Processing Systems,* edited by R. P. Lippmann, J. E. Moody, and D. J. Touretzky. San Mateo, CA: Morgan Kaufmann, 1991a, vol. 3, p. 39–45.

BROWN, T. H. AND ZADOR, A. M. Hippocampus. In: *The Synaptic Organization of the Brain,* (3rd ed.), edited by G. Shepherd. New York: Oxford Univ. Press, 1990, p. 346–388.

BROWN, T. H., ZADOR, A. M., MAINEN, Z. F., AND CLAIBORNE, B. J. Hebbian modifications in hippocampal neurons. In: *Long-Term Potentiation: A Debate of Current Issues,* edited by J. Davis and M. Baudry. Cambridge, MA: MIT Press, 1991b, p. 357–389.

BROWN, T. H., ZADOR, A. M., MAINEN, Z. F., AND CLAIBORNE, B. J. Hebbian computations in hippocampal dendrites and spines. In: *Single Neuron Computation,* edited by T. McKenna, J. Davis, and S. F. Zornetzer. San Diego, CA: Academic, 1992, p. 81–116.

BUTZ, E. G. AND COWAN, J. D. Transient potentials in dendritic systems of arbitrary geometry. *Biophys. J.* 14: 661–689, 1974.

CARNEVALE, N. T. AND JOHNSTON, D. Electrophysiological characterization of remote chemical synapses. *J. Neurophysiol.* 47: 606–621, 1982.

CARNEVALE, N. T. AND LEBEDA, F. J. Numerical analysis of electrotonus in multicompartmental neuron models. *J. Neurosci. Methods* 19: 69–87, 1987.

CARNEVALE, N. T., TSAI, K. Y., CLAIBORNE, B. J., AND BROWN, T. H. The electrotonic transformation: a tool for relating neuronal form to function. In: *Advances in Neural Information Processing Systems,* edited by G. Tesauro, D. Touretzky, and T. K. Leen. Cambridge, MA: MIT Press, 1995a, vol. 7, p. 69–76.

CARNEVALE, N. T., TSAI, K. Y., CLAIBORNE, B. J., AND BROWN, T. H. Qualitative electrotonic comparison of three classes of hippocampal neurons in the rat. In: *The Neurobiology of Computation: Proceedings of the Third Annual Computation and Neural Systems Conference,* edited by J. M. Bower. Boston, MA: Kluwer, 1995b, p. 67–72.

CARNEVALE, N. T., TSAI, K. Y., GONZALES, R., CLAIBORNE, B. J., AND BROWN, T. H. Biophysical accessibility of mossy fiber synapses on CA3 pyramidal cells. *Soc. Neurosci. Abstr.* 20: 715, 1994.

CAULLER, L. J. AND CONNORS, B. W. Functions of very distal dendrites: experimental and computational studies of layer I synapses on neocortical pyramidal cells. In: *Single Neuron Computation,* edited by T. McKenna, J. Davis, and S. F. Zornetzer. San Diego, CA: Academic, 1992, p. 199–230.

CLAIBORNE, B. J. The use of computers for the quantitative, three-dimensional analysis of dendritic trees. In: *Methods in Neuroscience, Computers and Computation in the Neurosciences,* edited by P. M. Conn. New York: Academic, 1992, vol. 10, p. 315–330.

CLAIBORNE, B. J., AMARAL, D. G., AND COWAN, W. M. A light and electron microscopic analysis of the mossy fibers of the rat dentate gyrus. *J. Comp. Neurol.* 246: 435–458, 1986.

CLAIBORNE, B. J., AMARAL, D. G., AND COWAN, W. M. Quantitative, three-dimensional analysis of granule cell dendrites in the rat dentate gyrus. *J. Comp. Neurol.* 302: 206–219, 1990.

CLAIBORNE, B. J., ZADOR, A. M., MAINEN, Z. F., AND BROWN, T. H. Computational models of hippocampal neurons. In: *Single Neuron Computation,* edited by T. McKenna, J. Davis, and S. F. Zornetzer. San Diego, CA: Academic, 1992, p. 61–79.

DESMOND, N. L. AND LEVY, W. B. Dendritic caliber and the 3/2 power relationship of dentate granule cells. *J. Comp. Neurol.* 227: 589–596, 1984.

EDWARDS, D. H., YEH, S.-R., ARNETT, L. D., AND NAGAPANN, P. R. Changes in synaptic integration during the growth of the lateral giant neuron of the crayfish. *J. Neurophysiol.* 72: 899–908, 1994.

FAULKNER, B., CHATTARJI, S., AND BROWN, T. H. Spontaneous synaptic currents in visualized neurons of the rat amygdala and perirhinal cortex. *Soc. Neurosci. Abstr.* 20: 1994.

FISHER, S. A., JAFFE, D. B., CLAIBORNE, B. J., AND BROWN, T. H. Self-organization of Hebbian synapses on a biophysical model of a hippocampal neuron. *Soc. Neurosci. Abstr.* 19: 808, 1993.

HARRIS, K. M., JENSEN, F. E., AND TSAO, B. Three-dimensional structure of dendritic spines and synapses in rat hippocampus (CA1) at postnatal day 15 and adult ages: implications for the maturation of synaptic physiology and long-term potentiation. *J. Neurosci.* 12: 2685–2705, 1992.

HARRIS, K. M. AND STEVENS, J. K. Dendritic spines of CA 1 pyramidal cells in the rat hippocampus: serial electron microscopy with reference to their biophysical characteristics. *J. Neurosci.* 9: 2982–2997, 1989.

HAÜSSER, M., STUART, G., RACCA, C., AND SAKMANN, B. Axonal initiation and active dendritic propagation of action potentials in substantia nigra neurons. *Neuron* 15: 637–647, 1995.

HEBB, D. O. *The Organization of Behavior.* New York: Wiley, 1949.

HILL, A. A. V., EDWARDS, D. H., AND MURPHY, R. K. The effect of neuronal growth on synaptic integration. *J. Comput. Neurosci.* 1: 239–254, 1994.

HILLMAN, D. E. Neuronal shape parameters and substructures as a basis of neuronal form. In: *The Neurosciences: Fourth Study Program,* edited by F. O. Schmitt and F. G. Worden. Cambridge, MA: MIT Press, 1979, p. 477–498.

HINES, M. Efficient computation of branched nerve equations. *Int. J. Biomed. Comput.* 15: 69–76, 1984.

HINES, M. A program for simulation of nerve equations with branching geometries. *Int. J. Biomed. Comput.* 24: 55–68, 1989.

HINES, M. NEURON—A program for simulation of nerve equations. In: *Neural Systems: Analysis and Modeling,* edited by F. Eeckman. Norwell, MA: Kluwer, 1993, p. 127–136.

HODGKIN, A. L. AND HUXLEY, A. F. A quantitative description of membrane current and its application to conduction and excitation in nerve. *J. Physiol. Lond.* 117: 500–544, 1952.

HOLMES, W. R. AND RALL, W. Electrotonic length estimates in neurons with dendritic tapering or somatic shunt. *J. Neurophysiol.* 68: 1421–1437, 1992a.

HOLMES, W. R. AND RALL, W. Estimating the electrotonic structure of neurons with compartmental models. *J. Neurophysiol.* 68: 1438–1452, 1992b.

HOLMES, W. R., SEGEV, I., AND RALL, W. Interpretation of time constant and electrotonic length estimates in multicylinder or branched neuronal structures. *J. Neurophysiol.* 68: 1401–1420, 1992.

ISHIZUKA, N., COWAN, W. M., AND AMARAL, D. G. A quantitative analysis of the dendritic organization of pyramidal cells in the rat hippocampus. *J. Comp. Neurol.* 362: 17–45, 1995.

JACK, J. J. B., NOBEL, D., AND TSIEN, R. W. *Electrical Current Flow in Excitable Cells.* London: Oxford Univ. Press, 1983.

JACOBS, G. A. AND NEVIN, R. Anatomical relationships between sensory afferent arborizations in the cricket cercal system. *Anat. Rec.* 231: 563–572, 1991.

JAFFE, D. B. AND BROWN, T. H. Confocal imaging of dendritic Ca^{2+} transients in hippocampal brain slices during simultaneous current-and voltage-clamp recording. *Microsc. Res. Tech.* 29: 279–289, 1994.

JAFFE, D. B., JOHNSTON, D., LASSER-ROSS, N., LISMAN, J. E., MIYAKAWA, H., AND ROSS, W. N. The spread of Na^+ spikes determines the pattern of dendritic Ca^{2+} entry into hippocampal neurons. *Nature Lond.* 357: 244–246, 1992.

JOHNSTON, D. Passive cable properties of hippocampal CA3 pyramidal neurons. *Cell. Mol. Neurobiol.* 1: 41–55, 1981.

JOHNSTON, D. AND BROWN, T. H. Interpretation of voltage-clamp measurements in hippocampal neurons. *J. Neurophysiol.* 50: 464–484, 1983.

JONAS, P., MAJOR, G., AND SAKMANN, B. Quantal components of unitary EPSCs at the mossy fibre synapse on CA3 pyramidal cells of rat hippocampus. *J. Physiol. Lond.* 472: 615–663, 1993.

KAIRISS, E. W., MAINEN, Z. F., CLAIBORNE, B. J., AND BROWN, T. H. Dendritic control of Hebbian computations. In: *Analysis and Modeling of Neural Systems,* edited by F. Eeckman. Boston, MA: Kluwer, 1992, p. 69–83.

KELSO, S. R., GANONG, A. H., AND BROWN, T. H. Hebbian synapses in hippocampus. *Proc. Natl. Acad. Sci. USA* 83: 5326–5330, 1986.

KOCH, C. AND SEGEV, I. (Editors). *Methods in Neuronal Modeling.* Cambridge, MA: MIT Press, 1989.

KOROGOD, S., BRAS, H., SARANA, V. N., GOGAN, P., AND TYC-DUMONT, S. Electrotonic clusters in the dendritic arborization of abducens motoneurons of the rat. *Eur. J. Neurosci.* 6: 1517–1527, 1994.

LARKMAN, A. U., MAJOR, G., STRATFORD, K. J., AND JACK, J. J. B. Dendritic morphology of pyramidal neurones of the visual cortex of the rat. IV. Electrical geometry. *J. Comp. Neurol.* 323: 153–166, 1992.

LORENTE DE NÓ, R. Studies on the structure of the cerebral cortex. II. Continuation of the study of the ammonic system. *J. Psychol. Neurol.* 46: 113–177, 1934.

MAGEE, J. C. AND JOHNSTON, D. Synaptic activation of voltage-gated channels in the dendrites of hippocampal pyramidal neurons. *Science Wash. DC* 268: 301–304, 1995.

MAINEN, Z. F., CLAIBORNE, B. J., AND BROWN, T. H. A novel role for synaptic competition in the development of cortical lamination. *Soc. Neurosci. Abstr.* 17: 759, 1991.

MAINEN, Z. F., ZADOR, A. M., CLAIBORNE, B. J., AND BROWN, T. H. Hebbian synapses induce feature mosaics in hippocampal dendrites. *Soc. Neurosci. Abstr.* 16: 492, 1990.

MAJOR, G., LARKMAN, A. U., JONAS, P., SAKMANN, B., AND JACK, J. J. B. Detailed passive cable models of whole-cell recorded CA3 pyramidal neurons in rat hippocampal slices. *J. Neurosci.* 14: 4613–4638, 1994.

MALINOW, R. AND MILLER, J. P. Postsynaptic hyperpolarization during conditioning reversibly blocks induction of long-term potentiation. *Nature Lond.* 320: 529–530, 1986.

MASCAGNI, M. V. Numerical methods for neuronal modeling. In: *Methods in Neuronal Modeling,* edited by C. Koch and I. Segev. Cambridge, MA: MIT Press, 1989, p. 439–484.

MCKENNA, T., DAVIS, J., AND ZORNETZER, S. F. (Editors). *Single Neuron Computation.* San Diego, CA: Academic, 1992.

NEVIN, R. H. W. *Morphological Analysis of Neurons in the Cricket Cercal System* (PhD dissertation). Berkeley, CA: Univ. of California, 1989.

O'BOYLE, M. P., RAHIMI, O., BROWN, T. H., AND CLAIBORNE, B. J. Im-

proved dendritic diameter measurements yield higher input resistances in modeled dentate granule neurons. *Soc. Neurosci. Abstr.* 19: 799, 1993.

PERKEL, D. H. AND MULLONEY, B. Calibrating compartmental models of neurons. *Am. J. Physiol.* 235 (*Regulatory Integrative Comp. Physiol.* 4): R93–R108, 1978.

RALL, W. Core conductor theory and cable properties of neurons. In: *Handbook of Physiology. The Nervous System. Cellular Biology of Neurons.* Bethesda, MD: Am. Physiol. Soc., 1977, sect. 1, vol. I, p. 39–97.

RALL, W., BURKE, R. E., HOLMES, W. R., JACK, J. J. B., REDMAN, S. J., AND SEGEV, I. Matching dendritic neuron models to experimental data. *Physiol. Rev.* 72: S159–S186, 1992.

RALL, W. AND RINZEL, J. Branch input resistance and steady attenuation for input to one branch of a dendritic neuron model. *Biophys. J.* 13: 648–688, 1973.

RIHN, L. L. AND CLAIBORNE, B. J. Dendritic growth and regression in rat dentate granule cells during late postnatal development. *Dev. Brain Res.* 54: 115–124, 1990.

SCHWINDT, P. C. AND CRILL, W. E. Amplification of synaptic current by persistent sodium conductance in apical dendrite of neocortical neurons. *J. Neurophysiol.* 74: 2220–2224, 1995.

SHEPHERD, G. M., BRAYTON, R. K., MILLER, J. F., SEGEV, I., RINZEL, J., AND RALL, W. Signal enhancement in distal cortical dendrites by means on interactions between active dendritic spines. *Proc. Natl. Acad. Sci. USA* 82: 2192–2195, 1985.

SHEPHERD, G. M. AND KOCH, C. Introduction to synaptic circuits. In: *The Synaptic Organization of the Brain* (3rd ed.), edited by G. Shepherd. New York: Oxford Univ. Press, 1990, p. 3–31.

SHEPHERD, G. M., WOLF, T. B., AND CARNEVALE, N. T. Comparisons of active properties of distal dendritic branches and spines; implications for neuronal computations. *J. Cognit. Neurosci.* 1: 273–286, 1989.

SILVER, R. A., TRAYNELIS, S. F., AND CULL-CANDY, S. G. Rapid time-course miniature and evoked excitatory currents at cerebellar synapses in situ. *Nature Lond.* 355: 163–166, 1992.

SPRUSTON, N., JAFFE, D., AND JOHNSTON, D. Dendritic attenuation of synaptic potentials and currents: the role of passive membrane properties. *Trends Neurosci.* 17: 161–166, 1994.

SPRUSTON, N., JAFFE, D., WILLIAMS, S. H., AND JOHNSTON, D. Voltage-and space-clamp errors associated with the measurement of electrotonically remote synaptic events. *J. Neurophysiol.* 70: 781–802, 1993.

SPRUSTON, N. AND JOHNSTON, D. Perforated patch-clamp analysis of the passive membrane properties of three classes of hippocampal neurons. *J. Neurophysiol.* 67: 508–529, 1992.

SPRUSTON, N., SCHILLER, Y., STUART, G., AND SAKMANN, B. Activity-dependent action potential invasion and calcium influx into hippocampal CA1 dendrites. *Science Wash. DC* 268: 297–300, 1995.

STALEY, K. J., OTIS, T. S., AND MODY, I. Membrane properties of dentate gyrus granule cells: comparison of sharp microelectrode and whole-cell recordings. *J. Neurophysiol.* 67: 1346–1358, 1992.

STRATFORD, K., MASON, A., LARKMAN, A., MAJOR, G., AND JACK, J. J. B. The modeling of pyramical neurones in the visual cortex. In: *The Computing Neuron,* edited by R. Durbin, C. Miall, and G. Mitchison. New York: Addison-Wesley, 1989, p. 296–321.

STERN, P., EDWARDS, F. A., AND SAKMANN, B. Fast and slow components of unitary EPSCs on stellate cells elicited by focal simulation in slices of rat visual cortex. *J. Physiol. Lond.* 449: 247–278, 1992.

STUART, G. AND SAKMANN, B. Active propagation of somatic action potentials into neocortical pyramidal cell dendrites. *Nature Lond.* 367: 69–72, 1994.

STUART, G. AND SAKMANN, B. Amplification of EPSPs by axosomatic sodium channels in neocortical pyramidal neurons. *Neuron* 15: 1065–1076, 1995.

THURBON, D., FIELD, A., AND REDMAN S. Electrotonic profiles of interneurons in stratum pyramidale of the CA1 region of rat hippocampus. *J. Neurophysiol.* 71: 1948–1958, 1994.

TRAUB, R. D. AND MILES, R. *Neuronal Networks of the Hippocampus.* Cambridge, UK: Cambridge Univ. Press, 1991.

TRUSSELL, L. O., ZHANG, S., AND RAMAN, I. M. Desensitization of AMPA receptors upon multiquantal neurotransmitter release. *Neuron* 10: 1185–1196, 1993.

TSAI, K. Y., CARNEVALE, N. T., AND BROWN, T. H. Hebbian learning is jointly controlled by electrotonic and input structure. *Network* 5: 1–19, 1994a.

TSAI, K. Y., CARNEVALE, N. T., CLAIBORNE, B. J., AND BROWN, T. H. Morphoelectrotonic transforms in these classes of rat hippocampal neurons. *Soc. Neurosci. Abstr.* 19: 1522, 1993.

TSAI, K. Y., CARNEVALE, N. T., CLAIBORNE, B. J., AND BROWN, T. H. Efficient mapping from neuroanatomical to electrotonic space. *Network* 5: 21–46, 1994b.

TURNER, D. A. Segmental cable evaluation of somatic transients in hippocampal neurons (CA1, CA3, and dentate). *Biophys. J.* 46: 73–84, 1984.

ULRICH, D., QUADRONI, R., AND LUSCHER, H.-R. Electrotonic structure of motoneurons in spinal cord slice cultures: a comparison of compartmental and equivalent cylinder models. *J. Neurophysiol.* 72: 861–871, 1994.

WIGSTROM, H., GUSTAFSSON, B., HUANG, Y.-Y., AND ABRAHAM, W. C. Hippocampal long-term potentiation is induced by pairing single afferent volleys with intracellularly injected depolarizing pulses. *Acta. Physiol. Scand.* 126: 317–319, 1986.

WIGSTROM, H., MCNAUGHTON, B. L., AND BARNES, C. A. Long-term synaptic enhancement in hippocampus is not regulated by postsynaptic membrane potential. *Brain Res.* 233: 195–199, 1982.

XIANG, Z., GREENWOOD, A. C., KAIRISS, E. W., AND BROWN, T. H. Quantal mechanisms of long-term potentiation in hippocampal mossy-fiber synapses. *J. Neurophysiol.* 71: 2552–2556, 1994.

YERAMIAN, E. AND CLAVERIE, P. Analysis of multiexponential functions without a hypothesis as to the number of components. *Nature Lond.* 326: 169–174, 1987.

ZADOR, A., HAGAI, A-S., AND SEGEV, I. The morphoelectrotonic transform: a graphical approach to dendritic function. *J. Neurosci.* 15: 1669–1682, 1995.